References

[1] Francke U, Arias DE, Nyham WL. Proximal 4p-deletion: phenotype differs from classical 4p-syndrome. J Pediatr 1977;90:250–2.

[2] White DM, Pillers DAM, Reiss JA, Brown MG, Magenis RE. Interstitial deletions of the short arm of chromosome 4 in patients with a similar combination of multiple minor anomalies and mental retardation. Am J Med Genet 1995;57:588–97.

[3] Chitayat D, Ruvalcaba RHA, Babul R, Teshima IE, Posnick JC, Vekemans MJJ, et al. Syndrome of proximal interstitial deletion 4p15: report of three cases and review of the literature. Am J Med Genet 1995;55:147–54.

[4] Uematsu M, Haginoya K, Kikuchi A, Nakayama T, Kakisaka Y, Numata Y, et al. Hypoperfusion in caudate nuclei in patients with brain-lung-thyroid syndrome. J Neurol Sci 2012;315:77–81.

[5] Saitsu H, Kato M, Mizuguchi T, Hamada K, Osaka H, Tohyama J, et al. *De novo* mutations in the gene encoding STXBP1 (MUNC18-1) cause early infantile epileptic encephalopathy. Nat Genet 2008;40:782–8.

[6] Nielsen J, Fischer O, Rasmussen K, Sillesen I, Bernsen A, Saldana-Garcia P. A 13-year-old girl with Wolf's syndrome and karyotype 46, XX, del(4)(pter integral p15::p12 integral qter),9qh+. Increased risk of structural chromosome abnormalities in the progeny of mothers with 9qh+. J Ment Defic Res 1977;21:119–26.

[7] Fryns JP, Yang A, Kleczkowska A, Lemmens F, Vandecasseye W, van den Berghe H. Interstitial deletion of the short arm of chromosome 4. A phenotype distinct from the Wolf-Hirschhorn syndrome. Ann Genet 1989;32:59–61.

[8] Ishikawa T, Sumi S, Fujimoto S, Shima Y, Wada Y. Interstitial deletion of the short arm of chromosome 4 in a boy with mild psychomotor retardation and dysmorphism. Clin Genet 1990;38:314–7.

[9] Davies J, Voullaire L, Bankier A. Interstitial deletion of the band 4p15.3 defined by sequential replication banding. Ann Genet 1990;33:92–5.

[10] Van de Graaf G, Sijstermans JMJ, Engelen JJM, Schrander-Stumpel CTRM. Mild phenotype in interstitial 4p deletion: another patient and review of the literature. Genet Couns 1997;8:13–8.

[11] Innes AM, Chudley AE, Carson NL, Dawson AJ. Interstitial 4p deletion in a child with an Angelman syndrome-like phenotype. Clin Genet 1999;56:238–41.

[12] Tonk VS, Jalal SM, Gonzalez J, Kennedy A, Velagaleti GVN. Familial interstitial deletion of chromosome 4 (p15.2p16.1). Ann Genet 2003;46:453–8.

[13] Kojima T, Mukai W, Fuma D, Ueda Y, Okada M, Sakaki Y, et al. Determination of genomic breakpoints in an epileptic patient using genotyping array. Biochem Biophys Res Commun 2006;341:792–6.

[14] Møller RS, Hansen CP, Jackson GD, Ullmann R, Ropers HH, Tommerup N, et al. Interstitial deletion of chromosome 4p associated with mild mental retardation, epilepsy and polymicrogyria of the left temporal lobe. Clin Genet 2007;72:593–8.

[15] Gawlik-Kuklinska K, Wierzba J, Wozniak A, Iliszko M, Debiec-Rychter M, Dubaniewicz-Wybieralska M, et al. Periventricular heterotopia in a boy with interstitial deletion of chromosome 4p. Eur J Med Genet 2008;51:165–71.

[16] Ray M, Evans J, Rockman-Greenberg C, Wickstrom D. Interstitial deletion of the short arm of chromosome 4. J Med Genet 1984;21:223–5.

[17] Romain DR, Columbano-Green LM, Parfitt RG, Chapman CJ, Smythe RH, Gebbie OB. A complex structural rearrangement of chromosome 4 in a woman without phenotypic features of Wolf-Hirschhorn syndrome. Clin Genet 1985;28:166–72.

[18] Gao F, Zhang Q, Zheng MH, Liu HL, Hu YY, Zhang P, et al. Transcription factor RBP-J-mediated signaling represses the differentiation of neural stem cells into intermediate neural progenitors. Mol Cell Neurosci 2009;40:442–50.

[19] Imayoshi I, Sakamoto M, Yamaguchi M, Mori K, Kageyama R. Essential roles of Notch signaling in maintenance of neural stem cells in developing and adult brains. J Neurosci 2010;30:3489–98.

[20] Hassed SJ, Wiley GB, Wang S, Lee JY, Li S, Xu W, et al. *RBPJ* mutations identified in two families affected by Adams-Oliver syndrome. Am J Hum Genet 2012;91:391–5.

Please cite this article in press as: Nakayama T et al. *RBPJ* is disrupted in a case of proximal 4p deletion syndrome with epilepsy.. Brain Dev (2013), http://dx.doi.org/10.1016/j.braindev.2013.07.009

ELSEVIER

Brain & Development xxx (2013) xxx–xxx

BRAIN & DEVELOPMENT
Official Journal of
the Japanese Society
of Child Neurology

www.elsevier.com/locate/braindev

Case report

Williams–Beuren syndrome with brain malformation and hypertrophic cardiomyopathy

Noriko Okamoto [a], Takanori Yamagata [a,*], Yukari Yada [a], Ko Ichihashi [a], Naomichi Matsumoto [b], Mariko Y. Momoi [a], Takeshi Mizuguchi [b]

[a] *Department of Pediatrics, Jichi Medical University, Japan*
[b] *Department of Human Genetics, Yokohama City University Graduate School of Medicine, Japan*

Received 3 March 2013; received in revised form 7 June 2013; accepted 4 July 2013

Abstract

Williams–Beuren syndrome (WBS) is a multisystemic genetic disorder caused by a contiguous gene deletion at 7q11.23. We report a severely affected WBS patient with cerebral and cerebellar dysplasia as well as hypertrophic cardiomyopathy. Microarray comparative genomic hybridization (aCGH) detected a deletion on 7q11.23 expanding from RP11-614D7 to RP11-137E8, which is a typical deletion in WBS. To the best of our knowledge, this is the first case report of a WBS patient with severe congenital central nervous system anomaly and progressive hypertrophic cardiomyopathy. The relationship between the genes deleted in WBS and a CNS anomaly plus hypertrophic cardiomyopathy requires further analysis.

© 2013 The Japanese Society of Child Neurology. Published by Elsevier B.V. All rights reserved.

Keywords: Williams syndrome; Cerebral and cerebellar dysplasia; Hypertrophic cardiomyopathy; Microarray comparative genomic hybridization analysis (aCGH)

---

1. Introduction

Williams–Beuren syndrome (WBS) is caused by a hemizygous deletion of chromosome 7q11.23 [1]. Phenotypes consist of characteristic facies, cardiovascular abnormalities, infantile hypercalcemia, growth deficiency, and intellectual disability. About 80% of patients have cardiovascular abnormalities, and supravalvular aortic stenosis (SVAS) is a characteristic feature [2]. With regard to neurological symptoms, mild microcephaly, intellectual disability, and personality disorders are common [3]. We report a patient with the common WBS deletion in 7q11.23 presenting with severe cerebral and cerebellar dysplasia and progressive hypertrophic cardiomyopathy. These phenotypes have not been previously reported.

2. Case report

The patient was born at 35 weeks of gestation with a weight of 2.294 kg (−0.16 standard deviation (SD)), a height of 42.5 cm (−1.2 SD), and a head circumference of 35.4 cm (+2.5 SD). The patient's dyspnea was controlled with mechanical ventilation. He had blepharophimosis, downward slanting of the palpebral fissure, strabismus, right iris hypopigmentation, a left pupillary membrane remnant, low-set ears, high-arched palate, periorbital fullness, broad nose, thick lips, wide mouth, micrognathia, loose skin, hypoplastic right toes with nail aplasia, deviation of the left second digit, and contracture of hip and knee joints. His voice was deep and

---

[*] Corresponding author. Address: Department of Pediatrics, Jichi Medical University School of Medicine, 3311-1, Yakushiji, Shimotsuke, Tochigi 329-0498, Japan. Tel.: +81 285 58 7366; fax: +81 285 44 6123.
E-mail address: takanori@jichi.ac.jp (T. Yamagata).

0387-7604/$ - see front matter © 2013 The Japanese Society of Child Neurology. Published by Elsevier B.V. All rights reserved.
http://dx.doi.org/10.1016/j.braindev.2013.07.002

Please cite this article in press as: Okamoto N et al. Williams–Beuren syndrome with brain malformation and hypertrophic cardiomyopathy. Brain Dev (2013), http://dx.doi.org/10.1016/j.braindev.2013.07.002

husky. Echocardiography on the day of birth revealed a small ventricular septal defect (VSD). At 1 month of age, right ventricular hypertrophy progressed and right ventricle outlet stenosis was detected. At 2 months of age, left ventricular hypertrophy and left ventricle output stenosis gradually progressed and severe mitral valve insufficiency was observed (Fig. 1d and e). Magnetic resonance imaging (MRI) at day 1 and day 81 after birth, and cranial computed tomography (CT) at 2 weeks of age showed dilatation of lateral and third ventricles, indicative of congenital hydrocephalus, thin cerebral cortex, hypoplasia of the cerebellum and brain stem, and agenesis of the corpus callosum (Fig. 1a–c). Beginning at 3 months of age, the patient had generalized tonic convulsions several times each day. Laboratory evaluation on the day of birth revealed mild hypocalcemia (7.8 mg/dl) and low blood sugar (34 mg/dl); both promptly improved with an intravenous infusion. Hypothyroidism was detected (free thyroxine (T4) 0.34 ng/dl (normal: 0.96–1.79 ng/dl); free triiodothyronine (T3) 1.18 pg/ml (normal: 2.47–4.34 pg/ml); and thyroid-stimulating hormone (TSH) 83.71 μIU/ml (normal: 0.34–3.5 μIU/ml)); thyroid hormone supplementation was initiated. His karyotype by G-banding was 46, XY. The auditory brainstem response showed bilateral hearing difficulties with the right threshold at 85 decibels (dB) and the left threshold at 105 dB. The patient died at 1 year and 5 months of age due to heart failure. At that time, his weight was 5.25 kg (−4.3 SD) and his height was 64 cm (−5.2 SD).

3. Materials and methods

3.1. Microarray CGH analysis (aCGH)

Comparative genomic hybridization analysis was performed using a custom BAC microarray containing 4219 BAC clones, as previously described [4]. In brief, after complete digestion using Dpn II, the subject's DNA was labeled with Cy-5 deoxycytidine triphosphate

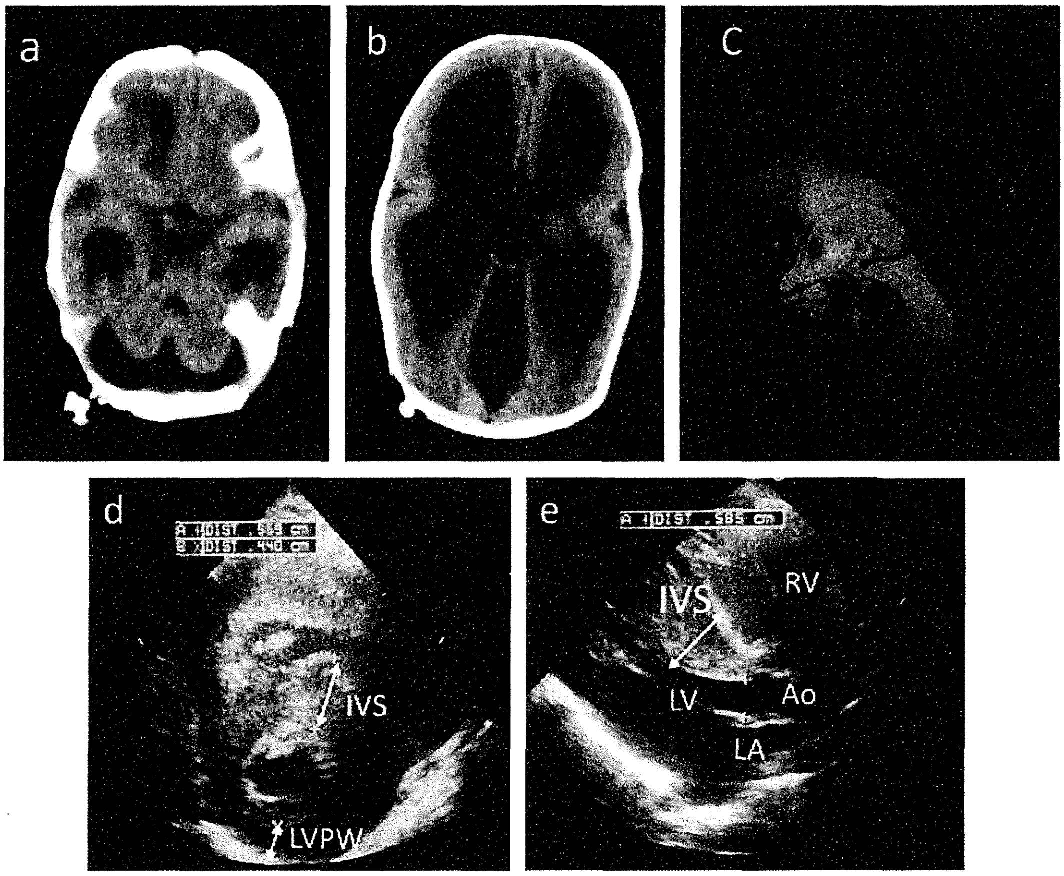

Fig. 1. Brain neuroimagings and echocardiogram. (1) Brain CT at 2 weeks of age (a, b) and T2-weighted imaging on MRI at day 1 (c) revealed dilated lateral and third ventricles, thin cerebral cortex, cerebellar hypoplasia, hypoplasia of brain stem, and agenesis of the corpus callosum. (2) Echocardiogram at 2 months of age (d, e) revealed hypertrophic obstructive cardiomyopathy with severe left ventricular outflow tract obstruction. Arrow indicates a markedly enlarged intraventricular septum (IVS). LVPW: posterior wall of left ventricle; LV: left ventricle; RV: right ventricle; LA: left atrium; Ao: aorta.

Please cite this article in press as: Okamoto N et al. Williams–Beuren syndrome with brain malformation and hypertrophic cardiomyopathy. Brain Dev (2013), http://dx.doi.org/10.1016/j.braindev.2013.07.002

(dCTP), and reference DNA was labeled with Cy-3 dCTP (Amersham Biosciences, Piscataway, NJ). Hybridization steps for array were preformed on a Tecan hybridization station HS400 (Tecan Japan, Kawasaki, Japan). Arrays were scanned by GenePix 4000B (Axon Instruments, Union City, CA) and analyzed using GenePix Pro 6.0 (Axon Instruments). The signal intensity ratio between patient and control DNA was calculated from the data of the single-slide experiment using the ratio of means formula (F635 mean − B635 median/F532 mean − B532 median) according to GenePix Pro 6.0. The standard deviation was calculated from the data of all clones.

3.2. Fluorescence in situ hybridization (FISH)

BAC DNAs, RP11-805G2 and RP11-359E24 were labeled with SpectrumGreen™ -11-deoxyuridine triphosphate (dUTP) or SpectrumOrange™ -11-dUTP (Vysis, Downers Grove, IL) by nick translation and denatured at 70 °C for 10 min. Probe-hybridization mixtures (15 l) were applied to the chromosomes, incubated at 37 °C for 16 h, then washed and mounted in antifade solution (Vector, Burlingame, CA) containing 4′-6′-diamidino-2-phenylindole.

These analyses were approved by the Bioethics Committee for human gene analysis at Jichi Medical University and Yokohama City University, and were performed after informed consent of patient's parents.

4. Results

With aCGH, a unique abnormality was detected: an approximate 1.0-Mb deletion in 7q11.23, ranging from RP11-614D7 (72,182,285–72,371,583) to RP11-137E8 (73,389,371–73,574,238) (Fig. 2a). This deletion range is commonly found in WBS. With FISH analysis, BAC clone RP11-805G2, which located within the deleted region, showed no signal on one of the 7q chromosome of the patient's lymphocytes. Instead, RP11-359E24, which located outside of the deletion, showed a signal (Fig. 2b). The patient's parents did not have

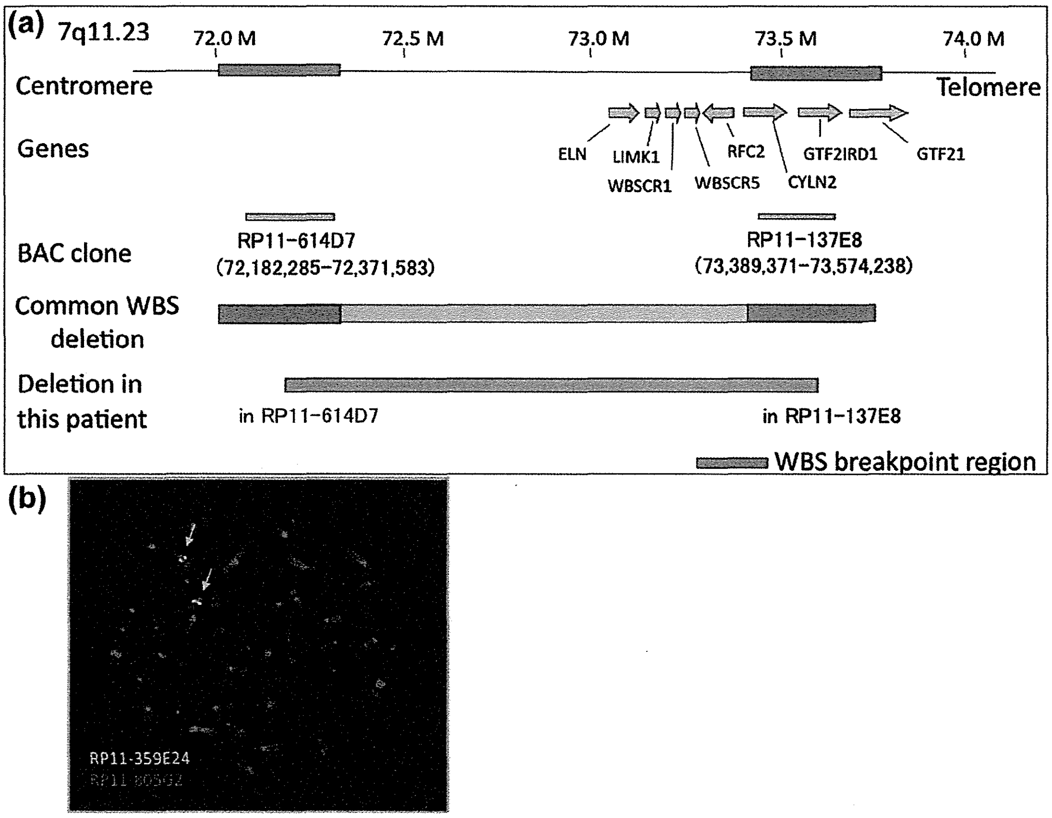

Fig. 2. (a) The range of the deletion detected in this case. Diagram presents a range of the common WBS deletion region and genes located nearby. The bar in the bottom indicates the extent of the deletion. In this case, aCGH detected the deletion expanding from RP11-614D7 to RP11-137E8. This interval of deletion is typical for WBS. (b) FISH analysis FISH results using BAC clone RP11-805G2 (red signal) localized in the common WBS deletion and RP11-359E24 (green signal) that is located outside of the deletion on chromosome 7 as probes. Our case had one normal chromosome 7 showing both green and red signals, and one chromosome 7 with a deletion missing a red signal. (For interpretation of the references to color in this figure legend, the reader is referred to the web version of this article.)

Please cite this article in press as: Okamoto N et al. Williams–Beuren syndrome with brain malformation and hypertrophic cardiomyopathy. Brain Dev (2013), http://dx.doi.org/10.1016/j.braindev.2013.07.002

Table 1
Clinical features of Williams Syndrome and our case.

Organ system	Problem	Williams syndrome	Our case
Facial	Combination of flat midface	Common	+
	Broad and depressed nasal bridge	CommonCommon	++
	Anteverted nares	Common	+
	Long philtrum	Common	+
	Thick lips	–	+
	High-arched palateLow-set ear	–	+
Ocular	Short palpebral fissures	50%	+
	Iris pigment abnormality	77%	+
	Strabismus	50%	+
Cardiovascular	Supravalvular aortic stenosis	64%	–
	Supravalvular pulmonic stenosis	24%	–
	Ventricular septal detect	12%5%	+–
	Patent ductus arteriosus	–	+
	Hypertrophic cardiomyopathy		
Central nervous system	Mild microcephaly	35%	–
	Mental retardation	95%	+
	Hypersensitivity to sound	90%	–
	Cerebellar hypoplasia	–	+
	Cerebral hypoplasia	–	+
	Infantile spasms	Rare	+
Musculoskeletal	Joint limitation	50%	+
	Joint contractures	Common	+
	Shift adhesion of digit	–	+
Gastrointestinal	Constipation	43%	–
Genitourinary	Renal artery narrowing	44%	–
Endocrine	Hypothyroidism	25%	+
Other findings	Hypoplastic, deeply set nails	65%	+
	Inguinal hernia	38%	+
	Umbilical hernia	14%	–
	Hypercalcemia	15%	–
	Hearing difficulties	NS	+

Modified from CA Morris et al. (1998) [2] and RJ Gorlin et al. (2001) [3]. +: present; –: absent.

the same deletion when tested by FISH analysis (data not shown).

5. Discussion

Clinical features of typical WBS and this case are compared in Table 1. Most of the common features of WBS were also observed in this case. In addition to these, some rare phenotypes of WBS, such as hearing difficulty and hypothyroidism [5], were detected. Conversely, SVAS, which is the most common cardiac anomaly associated with WBS [6], was not observed. Our patient developed rapidly progressing hypertrophic cardiomyopathy beginning at 2 months of age. A cardiomyopathy associated with WBS has been reported in only one 36-year-old patient [7], and severe hypertrophic cardiomyopathy has not been previously reported.

In addition, our patient exhibited the central nervous system (CNS) anomaly of congenital hydrocephalus and cerebral/cerebellar hypoplasia. Intellectual disabilities and behavioral problems are features of WBS; however, a CNS anomaly has not been previously noted as a clinical feature of WBS. Chiari I malformation has been reported in a small number of individuals with WBS [8], and parieto-occipital structural abnormality that might relate to visuospatial construction has been reported [9]. Schmitt et al. [10] reported that the midline lengths of the cerebral hemisphere and the corpus callosum were decreased in patients with WBS and suggested that the brain findings are consistent with aberrant premature termination of brain development. This proposed mechanism of premature termination of brain development might have occurred to a severe degree in this patient.

The extent of the deletion detected in this patient was typical of WBS; therefore, other specific genes that could explain these anomalies were not deleted. The possibility of the existence of some other gene mutation(s) in the homologous allele of the deleted region or outside of the deletion was not eliminated. It is possible that these anomalies could be features of WBS. There may be patients who remain undiagnosed because these features are atypical, and severe inducing early death. The relationships between the deleted genes in WBS and CNS anomalies as well as hypertrophic cardiomyopathies require further analysis.

Please cite this article in press as: Okamoto N et al. Williams–Beuren syndrome with brain malformation and hypertrophic cardiomyopathy. Brain Dev (2013), http://dx.doi.org/10.1016/j.braindev.2013.07.002

Acknowledgement

This work was supported in part by research grants from the Ministries of Education, Science and Culture, Japan.

References

[1] Nickerson E, Greenberg F, Keating MT, McCaskill C, Shaffer LG. Deletions of the elastin gene at 7q11.23 occur in approximately 90% of patients with Williams syndrome. Am J Hum Genet 1995;56:1156–61.

[2] Morris CA, Dilts C, Demsey SA, Leonard CO, Dilts C, Blackburn BL. The natural history of Williams syndrome: physical characteristics. J Pediatr 1988;113:318–26.

[3] Gorlin RJ, Cohen Jr MM, Hennekam RM. Syndromes of the head and neck. USA: Oxford University Press; 2001. p. 1032–8.

[4] Saitsu H, Kato M, Mizuguchi T, Hamada K, Osaka H, Tohyama J, et al. De novo mutations in the gene encoding STXBP1 (MUNC18-1) cause early infantile epileptic encephalopathy. Nat Genet 2008;40:782–8.

[5] Lashkari A, Smith AK, Graham JM. Williams–Beuren syndrome: an update and review for the primary physician. Clin Pediatr Phila 1999;38:189–208.

[6] Wessel A, Pankau R, Berdau W, Loens P. Aortic stiffness with the Williams–Beuren syndrome. Pediatr Cardiol 1997;18:244.

[7] Mäuser WS, Bonnemeier H. Cardiomyopathy and sudden cardiac death in Williams–Beuren syndrome. Int J Cardiol 2012;156:53–4.

[8] Pober BR, Filiano JJ. Association of Chiari I malformation in Williams syndrome. Pediatr Neurol 1995;12:84–8.

[9] Boddaert N, Mochel F, Meresse I, Seidenwurm D, Cachia A, Brunelle F, et al. Parieto-occipital grey matter abnormalities in children with Williams syndrome. Neuro Image 2006;30:721–5.

[10] Schmitt JE, Eliez S, Bellugi U, Reiss AL. Analysis of cerebral shape in Williams syndrome. Arch Neurol 2001;58:283–7.

Please cite this article in press as: Okamoto N et al. Williams–Beuren syndrome with brain malformation and hypertrophic cardiomyopathy. Brain Dev (2013), http://dx.doi.org/10.1016/j.braindev.2013.07.002

ELSEVIER

Brain & Development 35 (2013) 280–283

BRAIN & DEVELOPMENT
Official Journal of the Japanese Society of Child Neurology

www.elsevier.com/locate/braindev

Case report

Progressive diffuse brain atrophy in West syndrome with marked hypomyelination due to *SPTAN1* gene mutation

Yutaka Nonoda [a,*], Yoshiaki Saito [b], Shigehiro Nagai [b], Masayuki Sasaki [b], Toshiyuki Iwasaki [a], Naomichi Matsumoto [c], Masahiro Ishii [a], Hirotomo Saitsu [c]

[a] *Department of Pediatrics, School of Medicine, Kitasato University Hospital, Sagamihara, Japan*
[b] *Department of Child Neurology, National Center Hospital of Neurology and Psychiatry, National Center of Neurology and Psychiatry, Tokyo, Japan*
[c] *Department of Human Genetics, Yokohama City University Graduate School of Medicine, Yokohama, Japan*

Received 13 March 2012; received in revised form 4 May 2012; accepted 5 May 2012

Abstract

A 1-year-old male began suffering from West syndrome at 3 months of age, when electroencephalography revealed hypsarrhythmia accompanied by a periodic, brief suppression phase. The administration of adrenocorticotropic hormone was partially effective for stopping the condition, and the seizure type evolved into brief tonic seizures at 6 months. Thereafter, progressive atrophy of the brain became evident by 9 months of age, predominantly at the brainstem and cerebellum. Severe hypomyelination of the cerebral white matter was revealed at the age of 1 year, and a *de novo* heterozygous mutation in the *SPTAN1* gene was confirmed. The patient showed severely impaired psychomotor development, and had gained no visual attention. These findings contribute to the characterization of this recently established entity and facilitate the identification of further patients.
© 2012 The Japanese Society of Child Neurology. Published by Elsevier B.V. All rights reserved.

Keywords: West syndrome; Infantile spasm; Hypomyelination; Brainstem atrophy

1. Introduction

West syndrome is an epileptic syndrome with onset during infancy, characterized by a triad of the seizure phenotype of epileptic spasms, the finding of hypsarrhythmia on interictal electroencephalography (EEG), and psychomotor deterioration [1]. This condition results from various entities involving the developing brain, including dysplastic lesions, hypoxic-ischemic insults and metabolic disorders. Additionally, defects in certain genes have recently been identified in some cases of West syndrome without evidence of dysplastic or destructive brain lesions [2]. These include *SPTAN1*, a gene encoding α-II spectrin, which takes part in the clustering of sodium channels and has roles in the myelination process. Mutations or a deletion of the *SPTAN1* gene were revealed in three children who presented with early onset West syndrome and marked cerebral hypomyelination [3,4]. We experienced another patient with this condition, and herein want to delineate the clinical features, including the evolution of findings on EEG and neuroimaging, to further characterize the disorder.

2. Case report

A 1-year-old male was born to nonconsanguineous parents at 39 weeks of gestation with an Apgar score of 6 after an uneventful pregnancy. He had a birth

---

* Corresponding author. Address: Department of Pediatrics, Kitasato University Hospital, Kitasato 1-15-1, Minami-ku, Sagamihara, Kanagawa 252-0374, Japan. Tel.: +81 42 778 8111; fax: +81 42 778 8709.

E-mail address: nnd@med.kitasato-u.ac.jp (Y. Nonoda).

0387-7604/$ - see front matter © 2012 The Japanese Society of Child Neurology. Published by Elsevier B.V. All rights reserved.
http://dx.doi.org/10.1016/j.braindev.2012.05.002

weight 2886 g (−0.5SD), a body length 48.5 cm (−0.2SD) and a head circumference 31.5 cm (−1.0SD) at birth. He has three older siblings, who are all healthy. Laryngomalasia and an atrial septal defect were revealed during the neonatal period, and tube feeding was initiated at 1 month after birth due to failure to thrive. Electroencephalography (EEG) and magnetic resonance imaging (MRI; Fig. 1A, C and E) at this time showed unremarkable findings. Epileptic spasms emerged in series at the age of 3 months, when hypsarrhythmia was revealed on EEG (Fig. 2A). Notably, the epileptiform discharges with low synchrony often appeared periodically between interval periods of lower voltage amplitudes, showing an appearance similar to

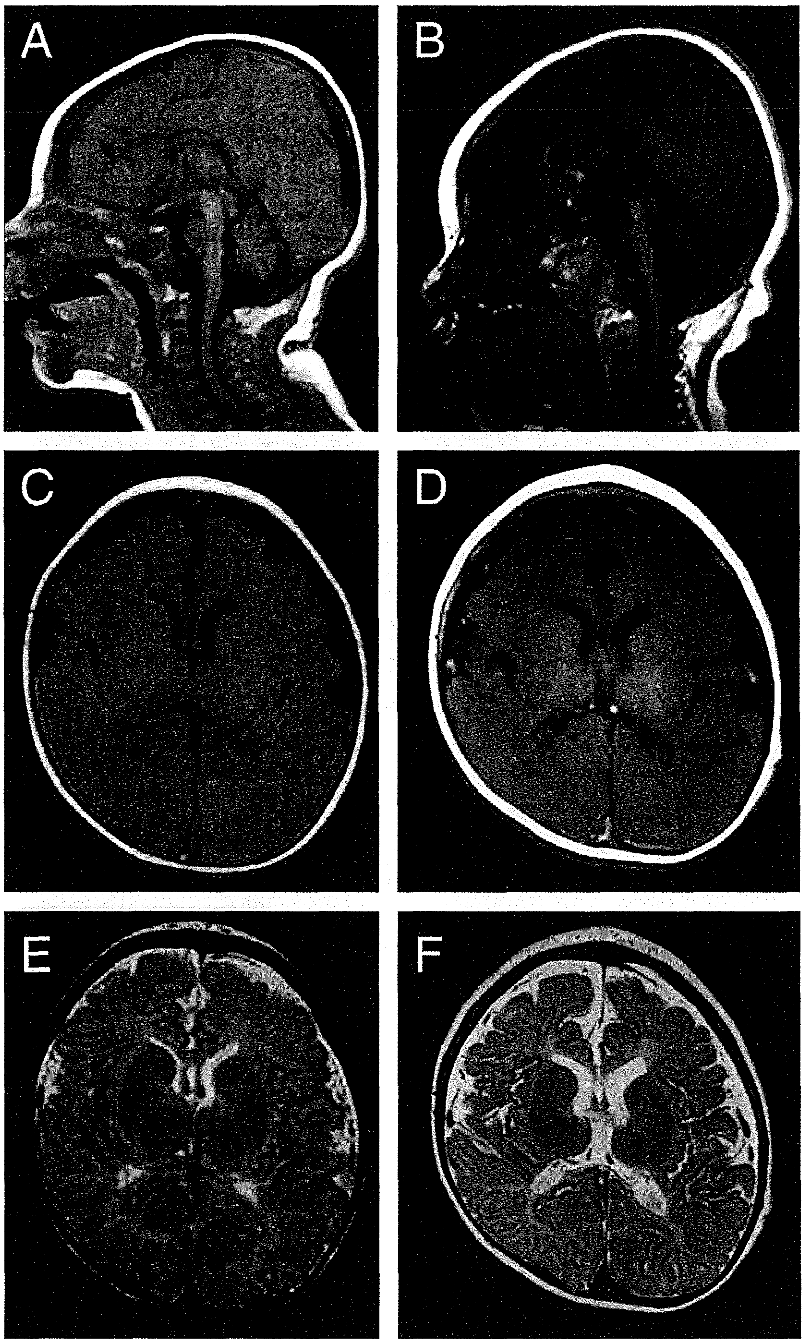

Fig. 1. Magnetic resonance imaging results of the patient ((A–D) T1-weighted images, (E and F) T2-weighted images) at the age of 2 months (A, C and E) and 1 year (B, D and F). Cerebral myelination did not proceed between these two periods, thus resulting in a marked hypomyelination at the age of 1 year. Note the diffuse brain atrophy at this latter period, which is most marked at the brainstem and cerebellum.

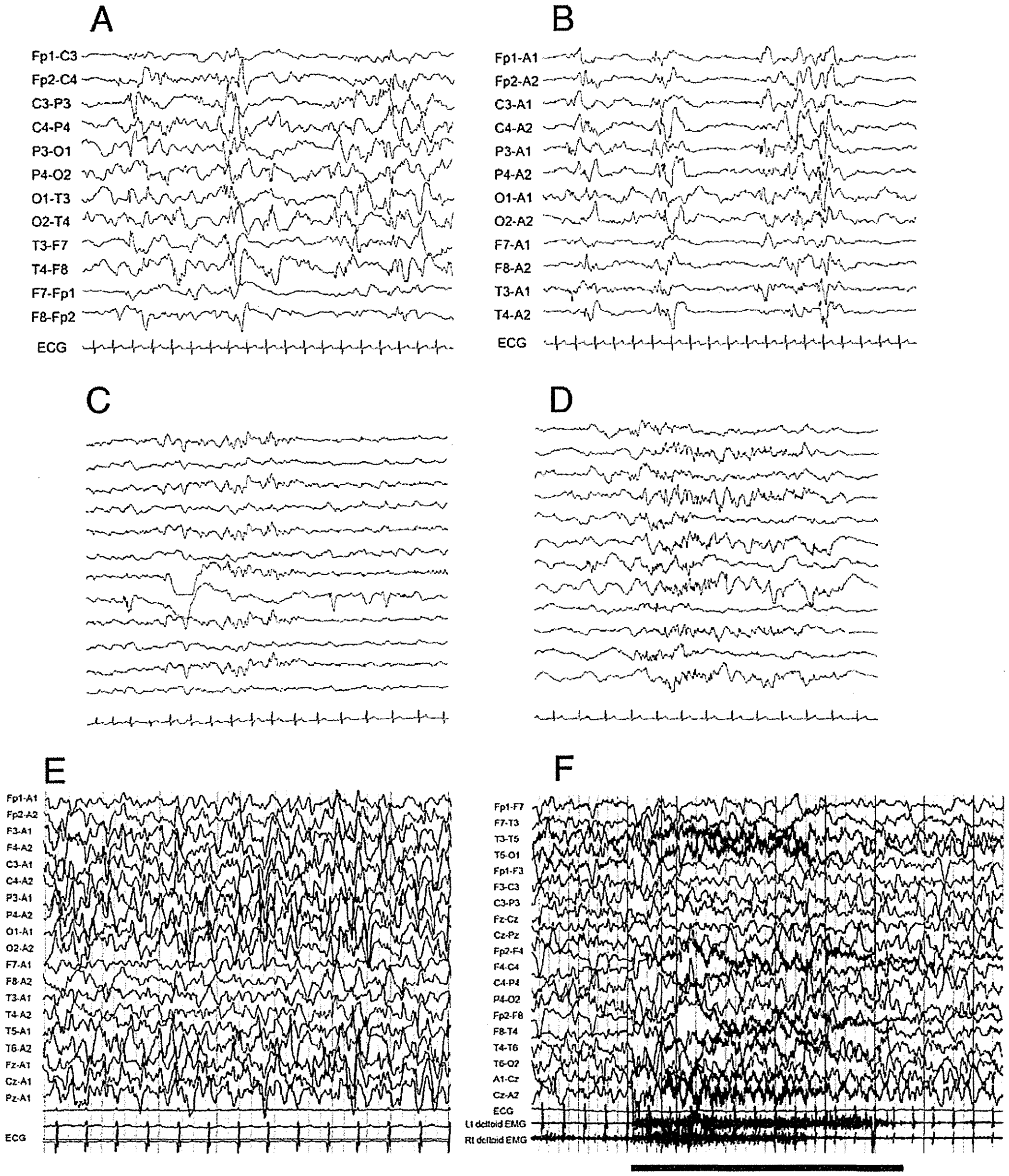
A
Fp1-C3
Fp2-C4
C3-P3
C4-P4
P3-O1
P4-O2
O1-T3
O2-T4
T3-F7
T4-F8
F7-Fp1
F8-Fp2
ECG
B
Fp1-A1
Fp2-A2
C3-A1
C4-A2
P3-A1
P4-A2
O1-A1
O2-A2
F7-A1
F8-A2
T3-A1
T4-A2
ECG
C
D
E
Fp1-A1
Fp2-A2
F3-A1
F4-A2
C3-A1
C4-A2
P3-A1
P4-A2
O1-A1
O2-A2
F7-A1
F8-A2
T3-A1
T4-A2
T5-A1
T6-A2
Fz-A1
Cz-A1
Pz-A1
ECG
F
Fp1-F7
F7-T3
T3-T5
T5-O1
Fp1-F3
F3-C3
C3-P3
Fz-Cz
Cz-Pz
Fp2-F4
F4-C4
C4-P4
P4-O2
Fp2-F8
F8-T4
T4-T6
T6-O2
A1-Cz
Cz-A2
ECG
Lt deltoid EMG
Rt deltoid EMG

Fig. 2. Electroencephalography (EEG) of the patient during sleep (A–E) and wakefulness (F) at the age of 3 (A and B), 7 (C), and 8 (D) months, and at 1 year (E and F). The hypsarrhythmia at the onset of West syndrome (A) often showed a periodic appearance with intervals of low voltage amplitude (B). In (F), no change in the EEG activity was noted during a versive movement (bar) of the neck to the right side.

the suppression-burst pattern (Fig. 2B). Despite treatment with vitamin B6, valproate sodium (VPA) and zonisamide, daily seizures of 10 series or more persisted. Brief tonic seizures with ocular deviation and versive movements to the right side also appeared at 4 months. The patient showed stagnated psychomotor development by this period, and never gained the ability to gaze or track objects, or to control his head. Phenobarbital was initiated, but was terminated due to the adverse effect of somnolence, and adrenocorticotropin (ACTH) at 0.005 mg/kg/day showed no effect. After the infant developed complications of gastroenteritis and bronchitis, the administration of ACTH at a dose of 0.025 mg/kg/day at 7 months produced partial effects on the seizure frequency and EEG findings (Fig. 2C). However, the epileptic discharges on EEG gradually became aggravated thereafter (Fig. 2D) under treatment with VPA and potassium bromide.

Computed tomography revealed the findings of cerebral atrophy (not shown), which was suspected to be a transient shrinkage due to the ACTH at that time. The epileptic spasms and tonic seizures disappeared by 9 months, when the patient manifested brief versive movements to the right or left side 10 times per day.

The addition of clobazam, zonisamide and phenobarbital showed no effects on these episodes. Video-monitoring EEG at 1 year showed diffuse, dysrhythmic activity, with multifocal spikes and slow waves during both wakefulness and sleep (Fig. 2E), which showed no change during the versive movements (Fig. 2F). These episodes were therefore proven to be paroxysmal dystonic posturing and not true epileptic seizures.

At 7 months, visual evoked potentials had shown poorly segregated potentials, and delayed latencies in brainstem auditory evoked potentials. Upon examination at 1 year of age, the patient presented with a weight of 7.9 kg (−1.6SD), height 69.4 cm (−2.1SD) and head circumference 41.5 cm (−3.2SD). He was bedridden due to rigospastic tetraplegia, moved his extremities upon painful stimulation, but did not show any responses to visual and auditory stimuli. MRI at that time revealed a progression of the diffuse atrophy of the brain, which was most marked at the brainstem and the cerebellum (Fig. 1B, D and F). In addition, severe hypomyelination of the cerebral white matter was found (Fig. 1D and F). An analysis of the *SPTAN1* gene as described in a previous report [4] identified an in-frame 9 bp duplication (c.6908_6916 dup; p.Asp2303_Leu2305dup) within the last spectrin repeat (Fig. 3). This mutation was absent in the parents of the patient, as well as in 250 Japanese control subjects.

3. Discussion

An initial MRI at the age of 2 months did not reveal specific findings of the *SPTAN1*-related epileptic encephalopathy, because the marked hypomyelination, which is the hallmark of this entity, was difficult to assess at this age. However, it became evident at late infancy, which enabled us to confirm the proper molecular diagnosis. In addition, the progressive nature of brain atrophy has not yet been recognized in previous reports on West syndrome with marked hypomyelination [3,4,6]. This may be another characteristic of this disorder, and may be confused with ACTH-related brain shrinkage, as occurred in the present case. The atrophy of the brainstem and cerebellum, which were common to the other patients [3,4] may provide a clue to differentiate the former from the latter. As for the EEG findings, the degree of the periodic appearance of hypsarrhythmia was beyond the sleep-modulated increase in synchrony usually seen in cases of West syndrome, and was reminiscent of the suppression-burst pattern in the early infantile epileptic encephalopathy (Ohtahara syndrome) [5]. We could find similar findings of hypsarrhythmia with prolonged suppression in a previously reported case [4; patient1], and this may also be characteristic in subjects with *SPTAN1* mutations.

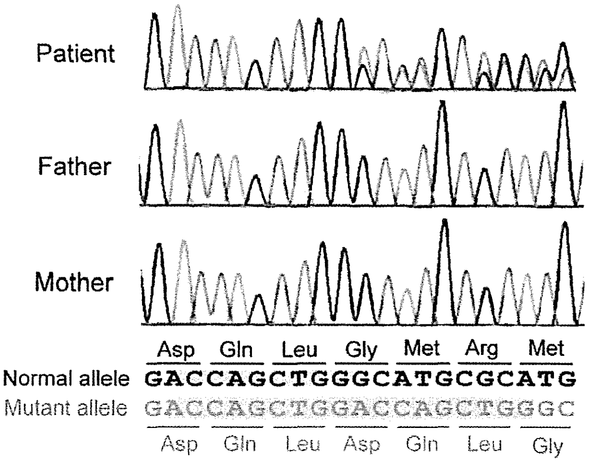

Fig. 3. The results of the genetic analysis. A direct sequence analysis of *SPTAN1* revealed a heterozygous c.6908_6916 dup (p.Asp2303_Leu2305dup) mutation, which occurred *de novo*, in the patient.

Therefore, the progressive atrophy of infratentorial structures and hypsarrhythmia with suppression phase may be additional hallmarks for further patients. In addition, not all patients with West syndrome and marked hypomyelination harbor *SPTAN1* mutations [4]. It should therefore be elucidated whether these characteristics could indicate the existence of a subgroup of *SPTAN1* mutants from other patient populations.

References

[1] Dulac O, Tuxhorn I. Infantile spasms and West syndrome. In: Rojer J, Bureau M, Genton P, Tassinari CA, Wolf P, editors. Epileptic syndromes in infancy, childhood and adolescence. Moontrogue: John Libbey Eurotext; 2005. p. 53–72.

[2] Paciorkowski AR, Thio LL, Dobyns WB. Genetic and biologic classification of infantile spasms. Pediatr Neurol 2011;45:355–67.

[3] Tohyama J, Akasaka N, Osaka H, Maegaki Y, Kato M, Saito N, et al. Early onset West syndrome with cerebral hypomyelination and reduced cerebral white matter. Brain Dev 2008;30:349–55.

[4] Saitsu H, Tohyama J, Kumada T, Egawa K, Hamada K, Okada I, et al. Dominant-negative mutations in alpha-II spectrin cause West syndrome with severe cerebral hypomyelination, spastic quadriplegia, and developmental delay. Am J Hum Genet 2010;86:881–91.

[5] Aicardi J, Ohtahara S. Severe neonatal epilepsies with suppression-burst pattern. In: Rojer J, Bureau M, Genton P, Tassinari CA, Wolf P, editors. Epileptic syndromes in infancy, childhood and adolescence. Moontrogue: John Libbey Eurotext; 2005. p. 39–50.

[6] Hamdan FF, Saitsu H, Nishiyama K, Gauthier J, Dobrzeniecka S, Spiegelman D, et al. Identification of a novel in-frame de novo mutation in *SPTAN1* in intellectual disability and pontocerebellar atrophy. Eur J Hum Genet 2012. http://dx.doi.org/10.1038/ejhg.2011.271.

CLINICAL REPORT

AMERICAN JOURNAL OF
medical genetics
PART A

A Case of Toriello–Carey Syndrome With Severe Congenital Tracheal Stenosis

Noritaka Yokoo,[1]* Chieko Marumo,[1] Yoshinobu Nishida,[1] Jun Iio,[1] Shinji Maeda,[1] Michiko Nonaka,[1] Toshiro Maihara,[1] Satoru Chujoh,[2] Tetsuo Katayama,[2] Hisanori Sakazaki,[3] Naomichi Matsumoto,[4] and Nobuhiko Okamoto[5]

[1]Department of Pediatrics, Hyogo Prefectural Tsukaguchi Hospital, Amagasaki, Hyogo, Japan

[2]Department of Pediatric Surgery, Hyogo Prefectural Tsukaguchi Hospital, Amagasaki, Hyogo, Japan

[3]Department of Pediatric Cardiology, Hyogo Prefectural Amagasaki Hospital, Amagasaki, Hyogo, Japan

[4]Department of Human Genetics, Yokohama City University Graduate School of Medicine, Yokohama, Kanagawa, Japan

[5]Department of Medical Genetics, Osaka Medical Center and Research Institute for Maternal and Children Health, Izumi, Osaka, Japan

Manuscript Received: 28 August 2012; Manuscript Accepted: 26 December 2012

Toriello–Carey syndrome is rare condition characterized by agenesis of the corpus callosum, the Pierre Robin sequence, and facial anomalies such as telecanthus, short palpebral fissures, and a small nose with anteverted nares [Toriello and Carey, 1988]. In addition, tracheal and laryngeal anomalies are common complications in patients with Toriello–Carey syndrome, and these anomalies can lead to death [Kataoka et al., 2003]. Congenital tracheal stenosis is a life-threatening condition with high mortality. Even if surgery is successful, several serious complications can result in a high risk of mortality. We describe a case of a Japanese boy with Toriello–Carey syndrome who had severe congenital tracheal stenosis, in whom surgical tracheal plasty was avoided because of adequate respiratory care, allowing the patient to be alive at 18 months of age.

© 2013 Wiley Periodicals, Inc.

Key words: Toriello–Carey syndrome; congenital tracheal stenosis; single nucleotide polymorphism array; corpus callosum agenesis; Pierre Robin sequence

How to Cite this Article:
Yokoo N, Marumo C, Nishida Y, Iio J, Maeda S, Nonaka M, Maihara T, Chujoh S, Katayama T, Sakazaki H, Matsumoto N, Okamoto N. 2013. A case of Toriello–Carey syndrome with severe congenital tracheal stenosis.
Am J Med Genet Part A 161A:2291–2293.

INTRODUCTION

Toriello–Carey syndrome (OMIM no. 218980) was first described by Toriello and Carey in 1988 and is characterized by agenesis of the corpus callosum, the Pierre Robin sequence, and facial anomalies such as telecanthus, short palpebral fissures, and a small nose with anteverted nares. This syndrome also includes cardiac defects, hypotonia, and tracheal and laryngeal anomalies, which are common complications. These anomalies can lead to death. Here, we describe a case of a Japanese boy with Toriello–Carey syndrome who had severe congenital tracheal stenosis. Surgical tracheal plasty was avoided in this patient because adequate respiratory care, and the patient is alive at 18 months of age.

CLINICAL REPORT

A 28-year-old G0P0 mother delivered a male neonate at 33 weeks of gestation by cesarean. Her family history was unremarkable. The pregnancy was complicated with hydramnios and intrauterine growth retardation. No apparent fetal abnormalities were detected by fetal ultrasound. The neonate's birth weight was 1,330 g (<10th centile) and Apgar scores were 3 and 7 at 1 and 5 min, respectively. The neonate developed central cyanosis, cried weakly, and presented with severe respiratory distress immediately after birth. Thus, we attempted intubation, which was very difficult because of micrognathia. After intubation, he was admitted to the neonatal intensive care unit (NICU) and mechanical ventilation was started. We had difficulty inserting the tracheal tube during intubation even though the smallest-sized (2.0-mm inner diameter) tracheal tube was used, which suggested that he had congenital tracheal stenosis. No laryngeal anomaly was apparent under direct laryngoscopy during the intubation.

---

*Correspondence to:
Noritaka Yokoo, 6-8-17 Minamitsukaguchi, Amagasaki, Hyogo 661-0012, Japan. E-mail: n_yokoo@f7.dion.ne.jp
Article first published online in Wiley Online Library (wileyonlinelibrary.com): 19 July 2013
DOI 10.1002/ajmg.a.35861

© 2013 Wiley Periodicals, Inc.

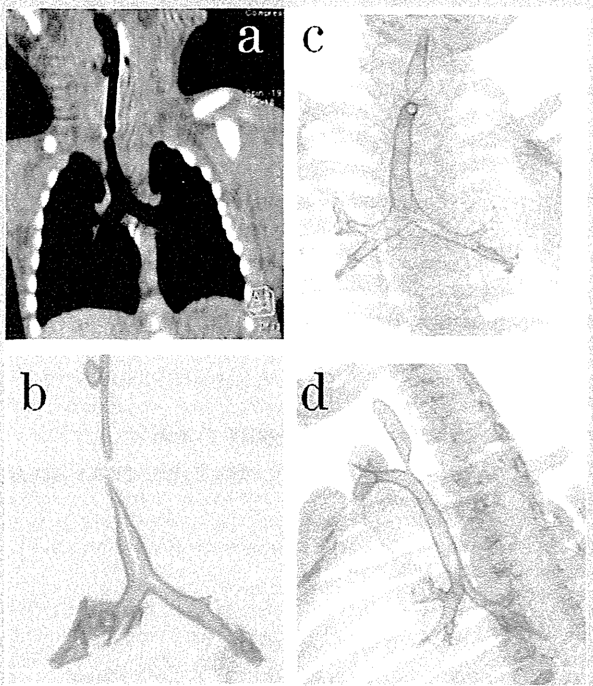

FIG. 1. a: Computed tomography (CT) on day 1. The patient's trachea is very narrow, and the outlet of the tracheal tube is nearly obstructed. b: Three-dimensional CT image of the trachea on day 1. The narrowest portion is not be visualized because of severe stenosis. c,d: Three-dimensional CT images of the trachea at 5 months. The trachea under the orifice has grown well, but the portion above the orifice is very narrow.

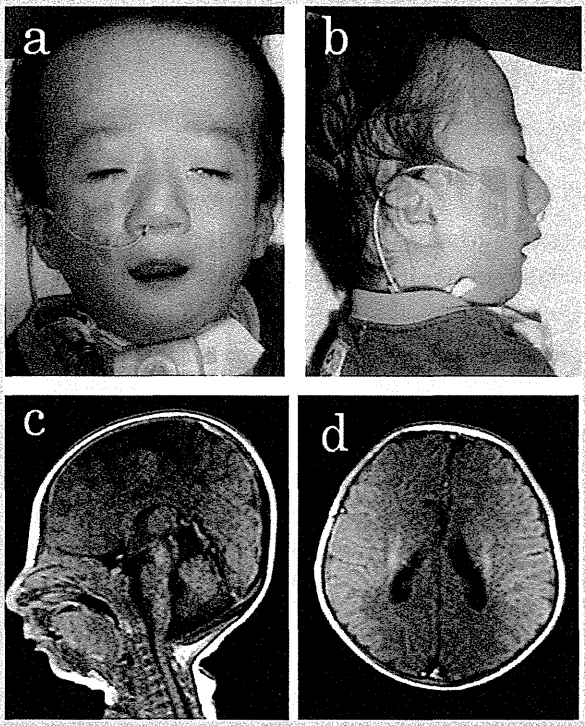

FIG. 2. a,b: The patient's face at 18 months of age. Note the short and downslanted palpebral fissures, small nose with anteverted nares, micrognathia, and low-set ears. c,d: Magnetic resonance imaging (MRI) of the brain, which revealed agenesis of the corpus callosum.

Cervical computed tomography (CT) on day 1 showed a stenosed trachea (Fig. 1a,b), and congenital tracheal stenosis was diagnosed. CT also showed that the tip of the tracheal tube was positioned just above the narrowest portion of the trachea. Thus, a tracheostomy was performed for securing the airway on day 2, and a tracheal tube with an inner diameter of 2.0 mm was inserted into the tracheostomy orifice. Mechanical ventilation was continued after tracheostomy.

In addition to congenital tracheal stenosis, several other anomalies were noted, including a large fontanelle, short and downslanted palpebral fissures, a small nose with anteverted nares, a high palate, micrognathia, cryptorchidism, and low-set ears (Fig. 2a,b). CT of the head revealed hypoplasia of the inner ears and magnetic resonance imaging (MRI) revealed agenesis of the corpus callosum (Fig. 2c,d). Echocardiography showed double-outlet right ventricle, infundibular pulmonary stenosis, and a ventricular septal defect. We diagnosed Toriello–Carey syndrome on the basis of these clinical features. His karyotype was 46 XY, and we assessed the chromosomes with single nucleotide polymorphism (SNP) array. SNP array revealed a 1.6-Mb duplication at 1q.31.2–31.3 and three deletions on chromosomes 8, 15, and 16. However of the three deletions normal variants that were previously described, duplication on chromosome 1 had not been reported. We further investigated the genes located on duplicated chromosome by quantitative polymerase chain reaction (qPCR) method, whose results revealed that this duplication was a normal variant (data not shown). In addition, his mother also had the same duplication of chromosome 1.

During hospitalization, the child's body weight increased because of tubal feeding. We determined that surgical repair for the tracheal stenosis would be difficult because of congenital heart disease. Hence, we serially increased the size of the tracheal tube according to his physical growth and mechanically dilated his trachea. Fortunately, his tracheal tube size could be increased and no adverse effects occurred. Ventilatory support was successfully withdrawn on day 57. The patient needed no ventilatory support except for a tracheostomy tube and was discharged on day 97.

The patient is now 18 months old. Except for several mild respiratory infections, he has experienced no airway problems after discharge from NICU. A three-dimensional CT image obtained at 5 months of age showed that the portion of the trachea below the tracheostomy site had grown well, but the trachea above the tracheal tube orifice remained very narrow (Fig. 1c,d). These CT images also showed that there was no pulmonary artery sling, which occasionally results in congenital tracheal stenosis. His ability to suck was so weak that tubal feeding needed to be continued. The congenital heart anomalies were well treated with a beta-blocker for preventing hypoxic spells because of the infundibular pulmonary stenosis. He had hearing impairment, poor vision, and severe growth and developmental retardation; his body weight was 5.6 kg (−4.2 - andard deviation [SD]), and his height was 69.3 cm (−3.9 SD). He was able to hold his head up at 10 months of age and roll over at 13 months of age, but could not sit up by himself. His skeletal muscles were moderately hypotonic. His developmental quotient at 18 months of age was 25 by the Kyoto Scale of Psychological Development, which is a standardized developmental test for Japanese children [Nakai et al., 2004].

DISCUSSION

Respiratory failure is the one of the most serious problems in patients with Toriello–Carey syndrome, particularly during the neonatal period, and they can lead to death [Kataoka et al., 2003]. Laryngeal and tracheal anomalies about Toriello–Carey syndrome have been reviewed [Toriello et al., 2003]. This patient had severe tracheal stenosis that would have caused death if no interventions were made. After the tracheostomy on day 2, adequate mechanical ventilation was provided. Fortunately, we were able to progressively increase the size of the tracheal tube. Cervical CT images performed at 5 months were very interesting. The portion of the trachea below the tracheostomy site had shown adequate growth, but the narrow portion above the tracheostomy site remained unchanged since birth. Thus, we were able to successfully dilate his trachea with serial increases in the size of tracheal tubes without adverse effects. A previous report noted that the mortality rate from congenital tracheal stenosis is 44–79% [Walker et al., 1992]. Surgery is the standard treatment for severe congenital tracheal stenosis [Chiu and Kim, 2006]. However, surgical intervention is usually associated with several serious complications, and children with congenital tracheal stenosis have the greatest risk of operative mortality [Peng et al., 2011]. A recent study showed the effectiveness of balloon dilatation and stent placement in patients with congenital tracheal stenosis [Xu et al., 2012]. Our strategy for treating the congenital tracheal stenosis was the same as balloon dilatation. In addition, placing a tracheal tube could prevent restenosis of his trachea similar to balloon dilatation and stent placement. Our patient had severe congenital tracheal stenosis, but we were able to avoid tracheal plasty with adequate respiratory care. He is alive at 18 months of age.

Several chromosomal abnormalities have been reported in patients with Toriello–Carey syndrome, not only by G-band staining or fluorescence in situ hybridization but also using the array comparative genomic hybridization (CGH) technique [McGoey et al., 2010; Said et al., 2011]. We investigated this patient's chromosomes by SNP array, which revealed no abnormalities. Further chromosome analyses on patients with Toriello–Carey syndrome should be performed.

In conclusion, we experienced a case of Toriello–Carey syndrome with severe congenital tracheal stenosis that was managed without surgical tracheal plasty.

REFERENCES

Chiu PP, Kim PC. 2006. Prognostic factors in the surgical treatment of congenital tracheal stenosis: A multicenter analysis of the literature. J Pediatr Surg 41:221–225.

Kataoka TR, Ito A, Nakabori T, Koma Y, Nakai H, Kamata S, Kitamura Y. 2003. Toriello–Carey syndrome associated with respiratory failure and non-mechanical ileus. Am J Med Genet Part A 120A:537–541.

McGoey R, Varma A, Lacassie Y. 2010. Siblings with phenotypic overlap with Toriello–Carey syndrome and complex cytogenetic imbalances including 3q29 microduplication and 6p25 microdeletion: Review of the literature and additional evidence for genetic heterogeneity. Am J Med Genet Part A 152A:3068–3073.

Nakai K, Suzuki K, Oka T, Murata K, Sakamoto M, Okamura K, Hosokawa T, Sakai T, Nakamura T, Saito Y, Kurokawa N, Kameo S, Satoh H. 2004. The Tohoku Study of Child Development: A cohort study of effects of perinatal exposures to methylmercury and environmentally persistent organic pollutants on neurobehavioral development in Japanese children. Tohoku J Exp Med 202:227–237.

Peng YY, Soong WJ, Lee YS, Tsao PC, Yang CF, Jeng MJ. 2011. Flexible bronchoscopy as a valuable diagnostic and therapeutic tool in pediatric intensive care patients: A report on 5 years of experience. Pediatr Pulmonol 46:1031–1037.

Said E, Cuschieri A, Vermeesch J, Fryns JP. 2011. Toriello–Carey syndrome with a 6 Mb interstitial deletion at 22q12 detected by array CGH. Am J Med Genet Part A 155A:1390–1392.

Toriello HV, Carey JC. 1988. Corpus callosum agenesis, facial anomalies, Robin sequence, and other anomalies: A new autosomal recessive syndrome? Am J Med Genet 31:17–23.

Toriello HV, Carey JC, Addor MC, Allen W, Burke L, Chun N, Dobyns W, Elias E, Gallagher R, Hordijk R, Hoyme G, Irons M, Jewett T, LeMerrer M, Lubinsky M, Martin R, McDonald-McGinn D, Neumann L, Newman W, Pauli R, Seaver L, Tsai A, Wargowsky D, Williams M, Zackai E. 2003. Toriello–Carey syndrome: Delineation and review. Am J Med Genet Part A 123A:84–90.

Walker LK, Wetzel RC, Haller JA Jr. 1992. Extracorporeal membrane oxygenation for perioperative support during congenital tracheal stenosis repair. Anesth Analg 75:825–829.

Xu X, Li D, Zhao S, Liu X, Feng Z, Ding H. 2012. Treatment of congenital tracheal stenosis by balloon-expandable metallic stents in paediatric intensive care unit. Interact Cardiovasc Thorac Surg 14: 548–550.

The Journal of Immunology

Y Chromosome–Linked B and NK Cell Deficiency in Mice

Shu-lan Sun,* Satoshi Horino,* Ari Itoh-Nakadai,† Takeshi Kawabe,* Atsuko Asao,* Takeshi Takahashi,‡ Takanori So,* Ryo Funayama,§ Motonari Kondo,¶ Hirotomo Saitsu,‖ Naomichi Matsumoto,‖ Keiko Nakayama,§ and Naoto Ishii*

There are no primary immunodeficiency diseases linked to the Y chromosome, because the Y chromosome does not contain any vital genes. We have established a novel mouse strain in which all males lack B and NK cells and have Peyer's patch defects. By 10 wk of age, 100% of the males had evident immunodeficiencies. Mating these immunodeficient males with wild-type females on two different genetic backgrounds for several generations demonstrated that the immunodeficiency is linked to the Y chromosome and is inherited in a Mendelian fashion. Although multicolor fluorescence in situ hybridization analysis showed that the Y chromosome in the mutant male mice was one third shorter than that in wild-type males, exome sequencing did not identify any significant gene mutations. The precise molecular mechanisms are still unknown. Bone marrow chimeric analyses demonstrated that an intrinsic abnormality in bone marrow hematopoietic cells causes the B and NK cell defects. Interestingly, fetal liver cells transplanted from the mutant male mice reconstituted B and NK cells in lymphocyte-deficient *Il2rg*$^{-/-}$ recipient mice, whereas adult bone marrow transplants did not. Transducing the EBF gene, a master transcription factor for B cell development, into mutant hematopoietic progenitor cells rescued B cell but not NK cell development both in vitro and in vivo. These Y chromosome–linked immunodeficient mice, which have preferential B and NK cell defects, may be a useful model of lymphocyte development.*
The Journal of Immunology, **2013, 190: 6209–6220.**

Most primary immunodeficiencies are inherited disorders. For example, mutations of the common cytokine receptor γ-chain (*Il2rg*) gene, which is located on the X chromosome, cause X-linked SCID, which is characterized by T and NK cell deficiencies and functionally impaired mature B cells. Mutations of the recombinase-activating genes *Rag1* and *Rag2* induce T and B cell deficiencies while retaining functional NK cells. These immunodeficiencies are caused by gene mutations on an autosome or an X chromosome (1, 2). No hereditary Y chromosome–linked immunodeficiencies have been reported in humans.

The Y chromosome is one of two chromosomes that pair with the X chromosome and determine sex in most mammals. The mouse Y chromosome is 16-Mb long and contains 54 genes; the human Y chromosome is 58-Mb long and encodes 86 genes. It is apparent that Y chromosomes do not contain genes essential for life, because females do not have the Y chromosome. Only two studies showed the male mice–specific disorder that is Y chromosome linked. One is Yaa (Y-linked autoimmune accelerator). Yaa mice develop a disease similar to systemic lupus erythematosus, and the incidence and onset are much higher in males than in their female littermates in certain mouse strains, including BXSB and MLR (3). Recent studies have shown that in Yaa mice, the part of the X chromosome pseudoautosomal region containing the *TLR7* gene is translocated onto the Y chromosome. Therefore, the duplication of TLR7, which may render B cells hypersensitive to self-Ags containing RNA, contributes to the BXSB strain's Y-linked autoimmune-prone phenotype. However, the *Yaa* mutation alone is not sufficient to induce autoimmune disease in C56BL/6 male mice; additional genetic mutations are required. In this context, the autoimmune disease associated with the *Yaa* mutation is not a Y-chromosomal Mendelian disease. Another study showed a mouse strain in which Vα14i NKT cell is absent in the male mice (4). However, they did not analyze the Y chromosome, so the mechanism of Y chromosome–linked NKT deficiency is still unknown.

B cells are lymphocytes that play a large role in humoral immune responses. Murine B cell development is initiated in the fetal liver cells and relocates to the bone marrow after birth. B cell development requires the coordinated efforts of transcription factors and cytokines, particularly IL-7 (5). IL-7 regulates early B cell transcription factor (EBF) expression in the adult bone marrow (6). EBF is a B cell–specific transcription factor that regulates crucial genes affecting B cell development, such as *λ5*, *Vpre B*, and *mb-1* (7, 8). EBF cooperates with E2A to positively regulate Pax5 expression. These transcription factors, along with PU.1, are indispensable for B cell development (9–11).

NK cells are a distinct lymphocyte subset with a central role in innate immunity (12). Early studies suggested that NK cells, like B cells and myeloid-lineage cells, develop primarily in the bone marrow. NK precursor (NKP) cells derived from hematopoietic stem cells (HSCs) give rise to immature NK (iNK) and then

---

*Department of Microbiology and Immunology, Tohoku University Graduate School of Medicine, Sendai 980-8575, Japan; †Department of Biochemistry, Tohoku University Graduate School of Medicine, Sendai 980-8575, Japan; ‡Central Institute for Experimental Animals, Kawasaki 210-0821, Japan; §Department of Cell Proliferation, Tohoku University Graduate School of Medicine, Sendai 980-8575, Japan; ¶Department of Immunology, Toho University School of Medicine, Tokyo 143-8540, Japan; and ‖Department of Human Genetics, Yokohama City University Graduate School of Medicine, Yokohama 236-0004, Japan

Received for publication January 31, 2013. Accepted for publication April 19, 2013.

This work was supported in part by a grant-in-aid for scientific research on priority areas from the Ministry of Education, Science, Sports and Culture of Japan, a grant-in-aid for scientific research on priority areas from the Japan Society for the Promotion of Science, and grants from the Japan Science and Technology Agency, the Sumitomo Foundation, the Uehara Memorial Foundation, the Novartis Foundation for the Promotion of Science, and the Yakult Bio-Science Foundation.

Address correspondence and reprint requests to Prof. Naoto Ishii, Department of Microbiology and Immunology, Tohoku University Graduate School of Medicine, 2-1 Seiryo-machi, Aoba-ku, Sendai 980-8575, Japan. E-mail address: ishiin@med.tohoku.ac.jp

Abbreviations used in this article: E, embryonic day; EBF, early B cell transcription factor; FISH, fluorescence in situ hybridization; HPC, hematopoietic progenitor cell; iNK, immature NK; NKP, NK precursor; PP, Peyer's patch; SCF, stem cell factor.

Copyright © 2013 by The American Association of Immunologists, Inc. 0022-1767/13/$16.00

www.jimmunol.org/cgi/doi/10.4049/jimmunol.1300303

mature NK cells. Several transcription factors, such as Ets-1, Id2, PU.1, Ikaros, T-bet, E4BP4, and Irf-2 are required for NK cell maturation (12–14). Among these, PU.1, Ikaros, and Ets-1 are critical for generating NKPs, and the other factors become involved after cells are committed to the NK cell lineage. For example, *Id2*$^{-/-}$ mice have normal numbers of NKP and iNK cells but significantly fewer mature NK cells (15). However, these factors are not necessarily specific to the NK lineage, because their individual deletions sometimes cause defects in other hematopoietic cell lineages.

In this study, we established a novel immunodeficient mouse strain characterized by Y chromosome–linked hereditary B and NK cell deficiencies. B and NK cells gradually diminished after 3 wk of age and disappeared by 10 wk of age in 100% of the males of this strain. B cell development was arrested at the prepro-B cell stage, and NKP cells were almost undetectable in these mutant mice. Although intensive genomic analyses failed to reveal the precise molecular mechanisms of this Y-linked lymphocyte deficiency, the mouse phenotype suggests that a mutation of one gene may cause B and NK cell deficiency without affecting T cell development. Therefore, this novel mouse strain may be a useful model for distinguishing the developmental processes of B, T, and NK cells, which are thought to derive from common lymphoid progenitor cells.

Materials and Methods

Mice

B cell–deficient mice on a C57BL/6N background were bred and maintained under specific pathogen-free conditions. Unless otherwise indicated, age-matched (3–20 wk old) and female littermates were used as controls. All procedures were performed according to protocols approved by Tohoku University's Institutional Committee for the Use and Care of Laboratory Animals.

Flow cytometry

Single-cell suspensions were prepared and cells immunostained as previously described (16). Dead cells were positively stained by propidium iodide and excluded from analysis. Lymphocyte suspensions from the spleen, bone marrow, peripheral blood, and fetal liver were incubated with a CD16/32 mAb (2.4G2) and stained for 30 min on ice with a combination of the following mouse-specific Abs: FITC-CD19 (6D5; BioLegend, San Diego, CA), PE–anti-IgM (eB121-15F9; eBioscience, San Diego, CA), PE-CD3 (eBio500A2; eBioscience), Pacific Blue-CD4 (RM4-5; BD Pharmingen, San Diego, CA), allophycocyanin-CD8 (53-6.7; BioLegend), FITC-CD11b (M1/70; BD Pharmingen), PE–anti-NK1.1 (PK136; BD Pharmingen), allophycocyanin–anti-B220 (RA3-6B2; BioLegend), FITC-CD90.2 (53-2.1; BD Pharmingen), FITC-CD43 (S7; BD Pharmingen), PE–anti-Ly5.1 (6c3; BioLegend), Pacific Blue-CD24 (M1/69; BioLegend), FITC-CD34 (RAM34; BD Pharmingen), allophycocyanin-CD117 (2B8; BioLegend), PE/Cy7–anti-Sca-1 (D7; BioLegend), Biotin-CD127 (A7R34; BioLegend), Biotin-CD122 (TM-β1; BioLegend), PE-CD5 (53-7.3; BD Pharmingen), FITC–Gr-1 (RB6-8C5; BD Pharmingen), PE-Ter119 (TER119; BioLegend), FITC-CD71 (RI7217; BioLegend), allophycocyanin-CD3 (145-2c11; BioLegend), and PE–anti-IgM (eB121-15F9; eBioscience). Biotinylated Abs were visualized by BD Horizon V450 streptavidin (BD Pharmingen). Samples were analyzed with an FACSCanto II or LSRFortessa system (BD Biosciences); data were analyzed with FlowJo flow cytometry analysis software (Tree Star).

Radioactive proliferation assay

Splenic T cells were first separated by CD90.2 Microbeads (Miltenyi Biotec, Bergisch Gladbach, Germany). A total of 1 × 10^5 cells was then seeded in the wells of a 96-well plate precoated with 10 μg/ml anti-mouse CD3e mAb (145-2C11) in a RPMI 1640 containing 10% FCS, 200 U/ml streptomycin, 200 U/ml penicillin, 50 μM 2-ME, and 1 μg/ml anti-mouse CD28 mAb. After 48 h stimulation, 1 μCi/well [^{3}H]thymidine was added, and the incorporation of [^{3}H]thymidine was measured by a γ-scintillation counter.

Real-time PCR

Prepro-B (B220$^+$CD43$^-$CD24$^-$Ly51$^-$) cells were purified from bone marrow cells using an FACSAria II cell sorter (BD Biosciences) and lysed with 1 ml TRIzol reagent (Invitrogen, Carlsbad, CA). Total RNA was purified from the cells. The cDNA was then synthesized with SuperScript Reverse Transcriptase and Random Primers (Invitrogen). The cDNA was then amplified over 40 cycles on a 7500 Real-time PCR system using SYBR Premix EXtaq (TaKaRa Bio, Shiga, Japan), ROX Reference DyeII (TaKaRa Bio), and primer sets. All samples were normalized to GAPDH. The PCR primers for E12, E47, EBF, PU.1, Id2, Ikaros, and GAPDH were as follows: E12 forward, 5′-GGGAGGAGAAAGAGGATGA-3′ and reverse, 5′-GCTCCGCCTTCTGCTCTG-3′; E47 forward, 5′-GGGAGGAGAAAGAGGATGA-3′ and reverse, 5′-CCGGTCCCTCAGGTCCTTC-3′; PU.1 forward, 5′-GAACAGATGCACGTCCTCGAT-3′ and reverse, 5′-GGGGACAAGGTTTGATAAGGGAA-3′; EBF forward, 5′-CTACAGCAATGGGATACGGAC-3′; reverse, 5′-TTTCAGGGTTCTTGTCTTGGC-3′; Id2 forward, 5′-CTCCAAGCTCAAGGAACTGG-3′ and reverse, 5′-ATTCAGATGCCTGCAAGGAC-3′; Ikaros forward, 5′-TGTGTCATCGGAGCGAGAG-3′ and reverse, 5′-GGAAGGCATCCTGCGAGTT-3′; and GAPDH forward, 5′-CCAGGTTGTCTCCTGCGACTT-3′ and reverse, 5′-CCTGTTGCTGTAGCCGTATTCA-3′.

Adoptive cell transfer

Bone marrow cells were extracted by a pressurized flow of sterile tissue-culture medium through femurs and tibias dissected from donor mice. Fetal liver cells were taken from female or male mice at embryonic day (E) 17.5. Recipient *Il2rg*$^{-/-}$ mice were irradiated with 5 Gy, and on the following day, 4 × 10^6 adult bone marrow cells or fetal liver cells were transplanted into recipients via the tail vein.

Purification of hematopoietic progenitor cells from bone marrow and fetal liver

Hematopoietic progenitor cells (HPCs) were purified from adult bone marrow or E17.5 fetal liver cells by staining with the following mouse-specific, biotinylated lineage markers: CD3, B220, TER119, Gr1, DX5, and CD11b. HPCs were negatively separated by anti-Biotin MicroBeads with auto MACS Columns (Miltenyi Biotec).

In vitro lymphopoiesis

HPCs collected from adult bone marrow or E17.5 fetal liver cells were cultured on OP9 stromal cells in α-MEM medium containing 20% FCS, 200 U/ml streptomycin, 200 U/ml penicillin, and 50 μM 2-ME or 7 d. For B cell development, the medium was supplemented with 5 ng/ml stem cell factor (SCF), 5 ng/ml Flt3 ligand, and 10 ng/ml IL-7; for NK cells, the medium was supplemented with 5 ng/ml SCF, 5 ng/ml Flt3 ligand, and 30 ng/ml IL-15.

Retroviral transduction

We produced a virus from a packaging cell line, PLAT-E, by transiently transfecting the MSCV-EBF-IRES-GFP plasmid (6) and MSCV-IRES-GFP as control using FuGENE transfection reagent (Roche, Madison, WI). HPCs from males (Ly5.2) or female littermates (Ly5.2) were cultured in RPMI 1640 containing 10% FCS, 200 U/ml streptomycin, 200 U/ml penicillin, and 50 μM 2-ME supplemented with mouse recombinant SCF (50 ng/ml), IL-6 (10 ng/ml), IL-3 (5ng/ml), FLT-3 ligand (5 ng/ml), and IL-7 (5 ng/ml). On the following day, the cells were transferred onto a RetroNectin-coated (TaKaRa Bio) plate in the presence of retroviral supernatant. For spin infection, the plate was centrifuged at 2000 × *g* at 32°C for 2 h once daily on days 1 and 2. Two days postinfection, the cells were washed and then transferred into irradiated Ly5.1 wild-type mice or cocultured on OP9 cells under B or NK cell differentiation conditions.

Statistical analysis

Statistical analysis was performed by Student *t* test. The p values < 0.05 were considered significant.

Results

Mutant male mice lack NK and B cells and Peyer's patches

In our mouse population, a novel mutant strain emerged spontaneously, in which all males lacked Peyer's patches (PP) and mated these males with wild-type female mice, we observed their offspring for the presence or absence of PPs. Although PPs in both the male and female offspring were visible from 4 to 6 wk after birth, PPs were completely lacking in the male offspring as they grew up to 10 wk old (Fig. 1A and data not shown). This indicated that the early PP compartmentalization process was normal in the male mice. Moreover, each male mouse had a normal number of lymph nodes, although the lymph nodes were abnormally small, and was outwardly normal in behavior, fertility, and appearance. To understand the characteristic of these mutant male mice, we analyzed hematopoietic cells in the spleen, peritoneal cavity, thymus, bone marrow, and peripheral blood. Interestingly, the males had virtually no B (B1 and B2) cells and also had significantly fewer NK cells (NK1.1^+CD3^-) than their female littermates (Fig. 1B, 1C). NK deficiency was also confirmed with a different NK cell marker (CD3^-DX5^+FcRεI$^-$) (data not shown). However, there were no differences in the absolute cell number of myeloid and erythroid populations in the bone marrow or of RBCs in the periphery (Fig. 1B, 1F, 1G). In addition, the absolute

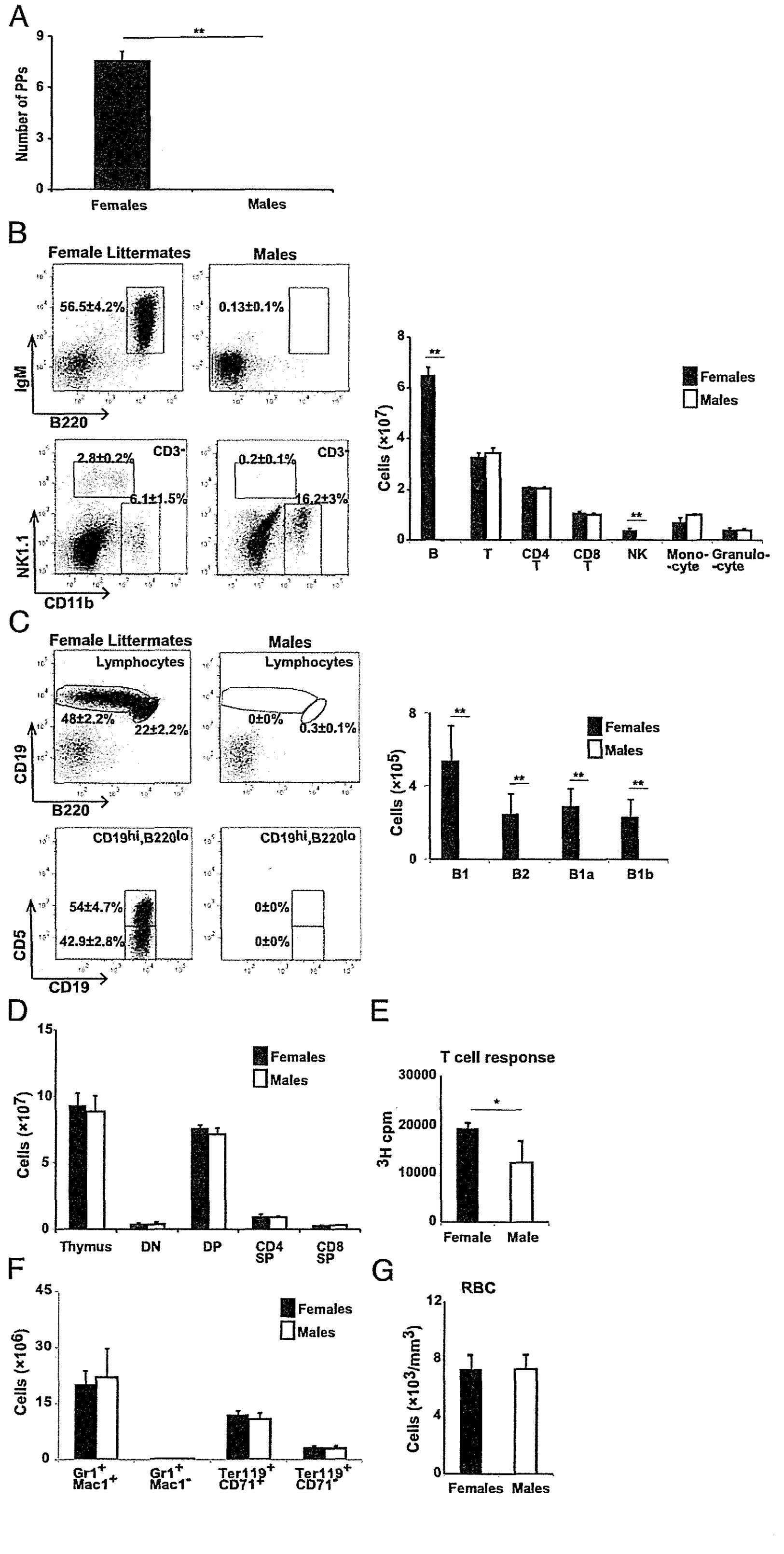

FIGURE 1. Mutant male mice specifically lack PPs. (**A**) Number of PPs on small intestines of 12-wk-old males or their female littermates. Frequency and the absolute number of hematopoietic lineages in the spleen (**B**), peritoneal cavity (**C**), thymus (**D**), and bone marrow (**F**) were analyzed by flow cytometry. B220^+IgM$^+$ B cell, CD3^+ T cell, CD3^+CD4^+ T cell, CD3^+CD8^+ T cell, NK1.1^+CD3^- NK cell, CD11b$^+$ monocyte, and Gr-1^+ granulocyte populations are shown. (C) Peritoneal lymphocytes were separated into the following subsets: total B1, CD19^+B$220^{\text{lo-int}}$; B1a, CD19^+B$220^{\text{lo-int}}$ D5^+; and B1b, CD19^+B$220^{\text{lo-int}}$ CD$5^{\text{lo}/-}$. (D) Thymic cells were stained with CD4 and CD8 and separated into the following subsets: double-negative (DN), CD4^-CD8^-; double-positive (DP), CD4^+CD8^+; CD4 single-positive (SP), CD4^+CD8^-; and CD8 SP, CD4^-CD8^+. (**E**) Splenic T cells were stimulated with anti-CD3 and anti-CD28 mAbs for 4–8 h and then pulsed with [^{3}H]thymidine. The incorporation of [^{3}H]thymidine was measured. (F) Myeloid cells (Gr1^+Mac1^+ and Gr1^+Mac1^-), Ter119^+CD71^+ nucleated erythroid progenitors, and Ter119^+ D71^- nonnucleated erythroid cells in the bone marrow were counted. (**G**) RBCs in the peripheral blood were counted. Numbers in FACS plots indicate the percentages relative to the gated cells. Data are from more than five experiments (A–D) or one experiment (E–G) with at least four mice per genotype. Error bars indicate SD (± SD). $*p < 0.05$, $**p < 0.01$.

number of T cell subsets in the thymus and spleen was comparable between the mutant males and the female littermate controls (Fig. 1B, 1D), suggesting normal T cell development in the mutant male mice. When splenic T cells were stimulated with anti-CD3ε mAb, the proliferative responses of T cells in the mutant male mice were clearly observed but significantly lower than female controls' (Fig. 1E).

B and NK cell deficiency is inherited in a Mendelian, Y chromosome–linked fashion

Because all male pups in this strain were B and NK cell deficient, we hypothesized that the phenotype might be inherited as a dominant trait linked to the Y chromosome. To confirm this, we mated PP (B and NK cell)–deficient male mice with wild-type female mice on a C57BL/6 (Fig. 2A, *left panel*) or BALB/c (Fig. 2A, *right panel*) background, and looked for PPs (B and NK cell) in their 10-wk-old offspring. All male offspring of a mutant male parent also lacked PPs (B and NK cells). In contrast, there was no abnormality in PPs or B cells in the female offspring or in males that inherited their Y chromosome from a wild-type male. The family tree indicated that the B and NK cell deficiency was inherited in a Mendelian fashion linked to the Y chromosome.

To determine the Y chromosome's genetic abnormality, we examined it by fluorescence in situ hybridization (FISH) analysis. The Y chromosome in the mutant males ($n = 10$) was one third shorter than that in wild-type male mice, suggesting a structural abnormality (Fig. 2B).

The Yaa mutation, which contributes to a higher incidence of autoimmune disease in male than in female BXSB mice, is caused by the novel translocation of a gene locus from the X chromosome onto the Y chromosome, resulting in the duplication of several genes. To look for duplication or copy-number abnormalities of certain genes in our B and NK cell–deficient male mice, we performed array-based comparative genomic hybridization with spleen cells and hepatic cells from mutant male and wild-type male mice on the same genetic background. We found gene-copy abnormalities of three autosomal gene loci (data not shown). However, FISH analysis with bacterial artificial chromosome clone probes derived from these three autosomal gene loci failed to find any evidence of an insertion or translocation of the loci into the Y chromosome (data not shown).

We also sequenced Y chromosome exomes from B and NK cell–deficient and wild-type male mice ($n = 3$ each) from the same B6 strain. However, we could not find any significant nucleotide differences, including single nucleotide polymorphisms, between the Y chromosome exons in mutant and wild-type mice (data not shown). Thus, the genetic Y chromosome abnormality responsible for the Y chromosome–linked immunodeficiency remains unclear.

B and NK cell populations in the mutant male mice decrease with age

B and NK cells were absent in the adult male mice of this strain. To examine whether B or NK cell lymphopenia occurs at birth, we measured the numbers of B and NK cells in the bone marrow, spleen, lymph nodes, and peripheral blood at 3, 6, 8, and 12 wk of age. The B and NK cell populations in males at 3 wk of age were comparable with those in females, but had decreased to a markedly lower level at 6 wk of age (Fig. 3A). Interestingly, B1 cells in the males were markedly reduced compared with those in the female littermates even at 3 wk after birth and completely disappeared by 12 wk of age (Fig. 3B). Consistent with B cell decline, serum IgG and IgM dramatically decreased at 6 wk of age (Fig. 3D). In contrast, T cells increased with age in both males and females and the thymic development of T cells in the males was normal (Fig. 3A, 3C).

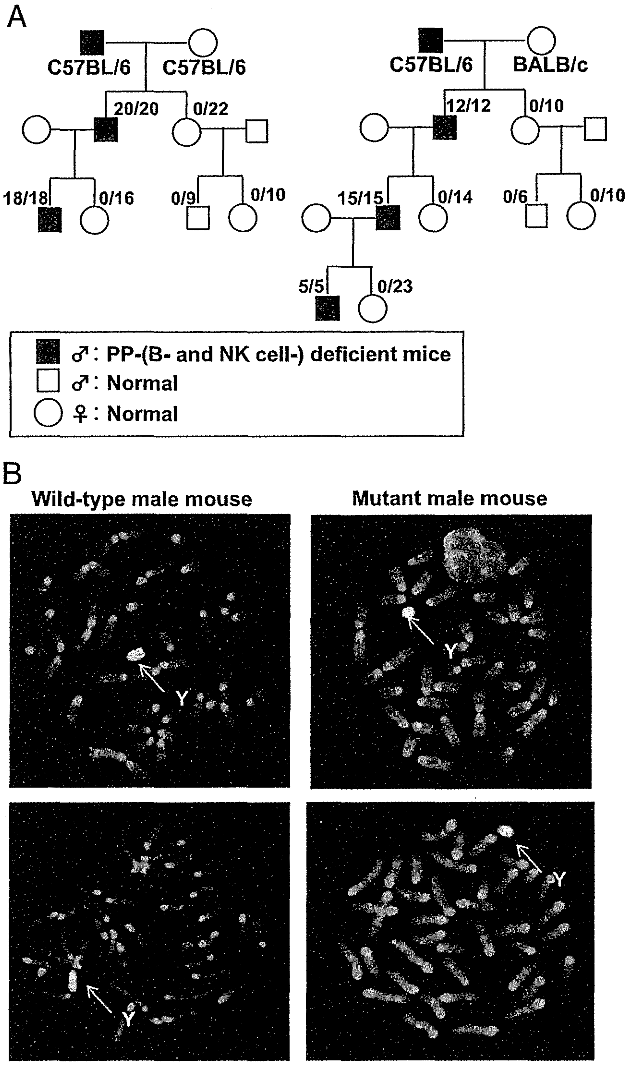

FIGURE 2. B and NK cell deficiency is inherited in a Mendelian fashion linked to the Y chromosome. (**A**) B cell–deficient male mice were mated with C57BL/6 (*left panel*) or BABL/c (*right panel*) wild-type female mice for several generations. The 10-wk-old offspring were then examined for B and NK cells in the peripheral blood and for PPs. Mice deficient in PPs (B and NK cells) are represented by filled symbols and unaffected individuals by open symbols (squares, males; circles, females). The numbers of immunodeficient mice/number of offspring are shown. (**B**) Y chromosomes from wild-type and B and NK cell–deficient males were analyzed by FISH. The Y chromosome is presented in yellow; pictures show Y chromosomes from different cells. Representative results are shown ($n = 20$ cells each).

To rule out the possibility that androgenic hormones were associated with this phenotype, we compared splenic B and T cells in 10-wk-old B cell–deficient males that had been either castrated or subjected to a sham operation at 2 wk of age (Fig. 3D). The castrated male mice lacked B cells but had normal T cells, indicating that the male-specific B cell defect was independent of androgen.

Bone marrow lymphopoiesis in the mutant male mice is arrested at the prepro-B to pro-B cell transition

Because B cells were depleted in the adult male mutant mice, we looked at various stages of B cell differentiation to determine which stage was arrested. The B cell development from HSCs is sub-

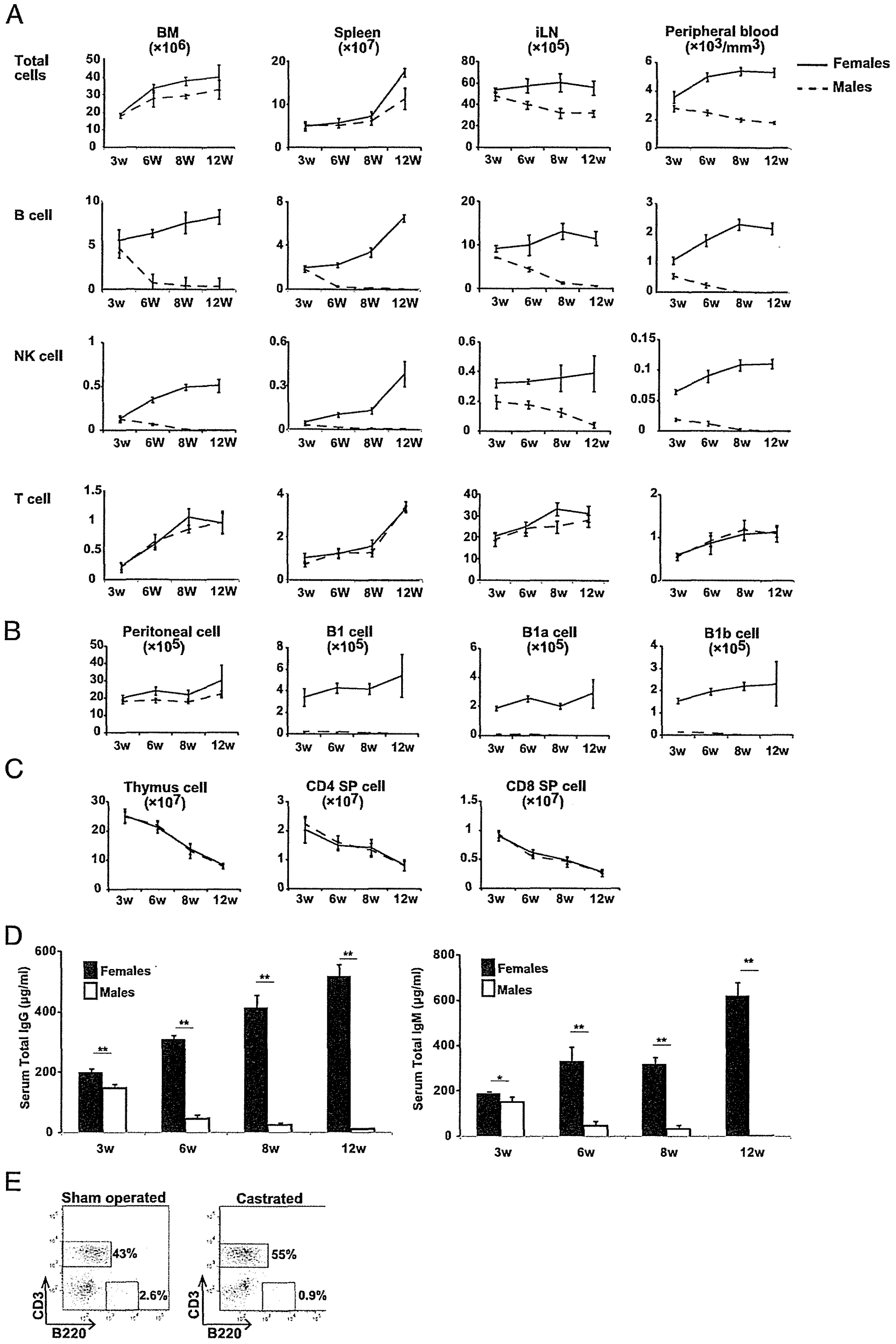

FIGURE 3. B and NK cell deficiencies are restricted to adults and are not affected by androgens. (**A**) Number of B cells (B220$^+$), T cells (CD3$^+$), and NK cells (NK1.1$^+$ CD3$^-$) from the bone marrow, spleen, inguinal lymph nodes (iLN), and blood. Numbers of B cell subsets in the peritoneal cavity (**B**) and number of T cell subset in the thymus (**C**) of male and female littermates at 3, 6, 8, and 12 wk of age. (**D**) Serum levels of IgG and IgM in 3-, 6-, 8-, and 12-wk-old mice were calculated from absorbance at 450 nm (A_{450}). Data are from one experiment ($n = 4$ mice/genotype). Error bars indicate SD (± SD). (**E**) The 2-wk-old male offspring of B cell–deficient male mice were castrated or subjected to a sham operation, and then the percentages of B and T cells in the spleen were compared at 10 wk of age. Data are from one experiment ($n = 2$ mice/group). $*p < 0.05$, $**p < 0.01$.

divided into Hardy fractions A–F (17). We found decreased numbers of B cell progenitors in the bone marrow that had undergone the transition from prepro-B to pro-B cells, corresponding to the Hardy fractions A (B220$^+$CD43$^+$BP-1$^-$CD24$^-$) and B (B220$^+$CD43$^+$BP-1$^-$CD24$^+$). Immature B cells, corresponding to Hardy fraction E (B220$^+$CD43$^-$IgM$^-$IgD$^+$), were severely deficient (Fig. 4A, 4B).

NK cells are lost in the mutant male mice

NK cells, which develop primarily in the bone marrow, are derived from HSCs via NKP and iNK cells. Because the very low number of splenic NKs in the mutant males suggested defective NK development, we compared the number of NKP and iNK cells in the bone marrow of males and their female littermates. The numbers of both NKP (CD11b$^-$CD3$^-$NK1.1$^-$CD122$^+$) and iNK (CD11b$^-$CD3$^-$NK1.1$^+$CD122$^+$) cells were substantially reduced in the male mice (Fig. 4C, 4D), suggesting that NK cell development was impaired in the males.

Abnormal expression of Sca-1 on hematopoietic cells in the bone marrow

We further examined the lymphoid, myeloid, and erythroid progenitor populations in the bone marrow of the mutant male mice. As shown in Fig. 5, it appeared that progenitor cells (defined as lineage$^-$c-Kit^{hi} and Sca-1$^-$) of all of the indicated lineages in the mutant males were markedly reduced. However, Fig. 1B and 1F showed normal number of mature myeloid and erythroid cells in the mutant male mice. Interestingly, most lineage$^-$ cells in the mutant males strongly expressed the Sca-1 marker (*top panels* of Fig. 5A), which is commonly used to define the hematopoietic

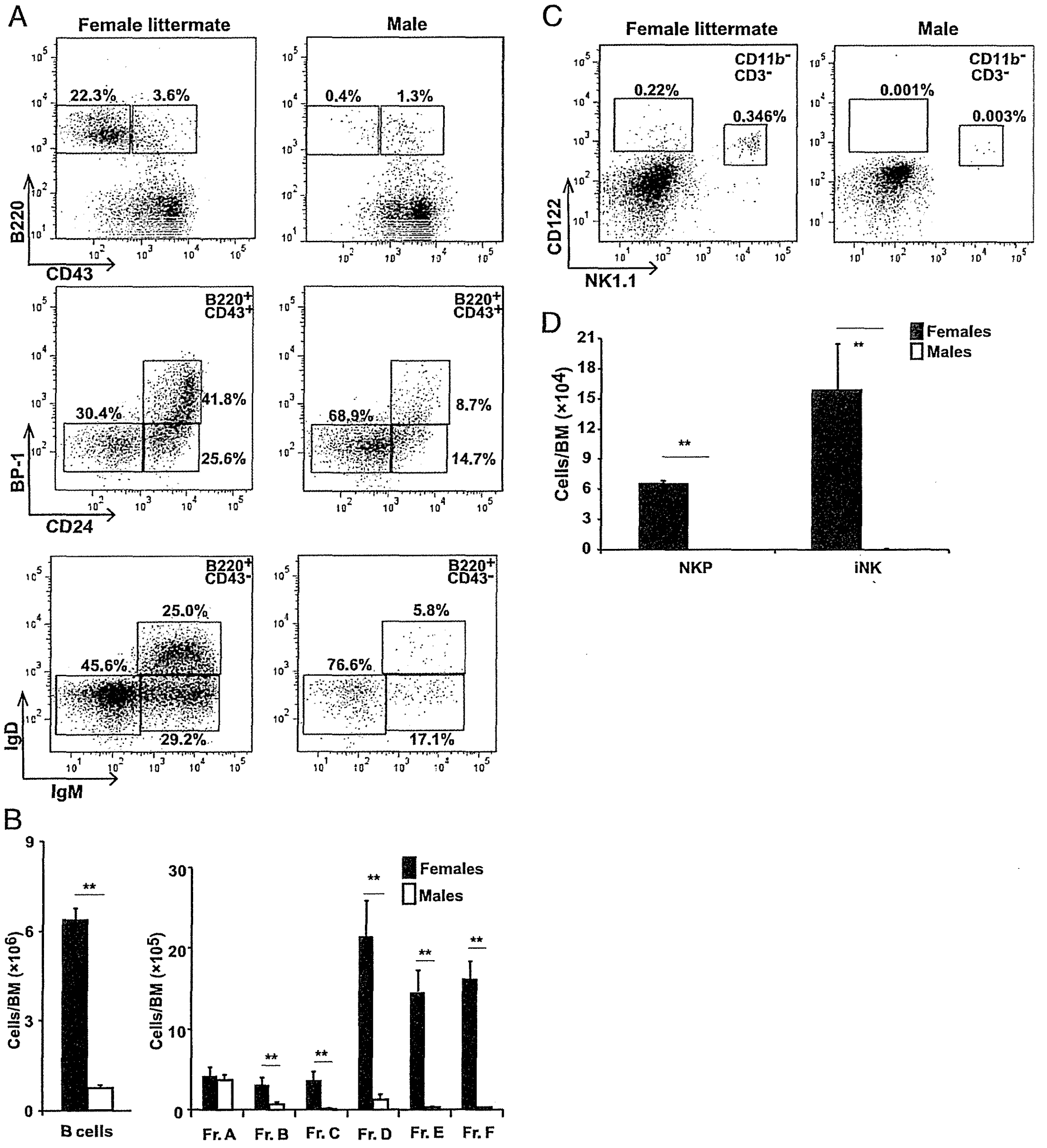

FIGURE 4. B and NK cell developments are arrested. Frequency (**A**) and number (**B**) of B cell subsets in the bone marrow at 6 wk of age. Hardy fractions in the bone marrow were gated as follows: B220$^+$CD43$^+$BP-1$^-$CD24$^-$ (A); B220$^+$CD43$^+$BP-1$^-$CD24$^+$ (A); B220$^+$CD43$^+$BP-1$^+$CD24$^+$ (A); B220$^+$CD43$^-$IgM$^-$IgD$^-$ (A); B220$^+$CD43$^-$IgM$^+$IgD$^-$ (A; and B220$^+$CD43$^-$IgM$^+$IgD$^+$ (B); the C' fraction (B220$^+$CD43$^+$BP-1$^+$CD24^{hi}) was not resolved. Data are representative from three independent experiments of five mice per genotype. Frequency (**C**) and number (**D**) of NKp (CD122$^+$CD3$^-$CD11b$^-$NK1.1$^-$) and iNK cells (CD122$^+$NK1.1$^+$CD3$^-$CD11b$^-$) are shown. Data are representative of four or five mice per genotype. **$p < 0.01$.

progenitor or stem cells. Therefore, due to abnormally high expression of Sca-1, we may have been unable to exactly evaluate the hematopoietic progenitor cells in the mutant male mice.

The failure of adult B and NK lymphopoiesis is cell intrinsic

B cells and NK cells can be produced from bone marrow cells cultured in vitro on stromal cells, such as OP9 cells, in the presence of IL-7 or IL-15 (18, 19). To determine the cellular origin of the phenotype of the male mutant mice, we isolated HPCs, identified as Lin$^-$ (B220$^-$, Thy1$^-$, DX5$^-$, Ter119$^-$, Gr-1$^-$, CD11b$^-$) bone marrow cells, from the male mice and their female littermates. The HPCs were cultured on OP9 cells, with subsequently added cytokines. HPCs derived from the bone marrow of males did not produce NK (NK1.1$^+$) cells or B (CD19$^+$) cells, whereas significant NK and B cell populations were generated from the HPCs from female littermates (Fig. 6A).

To confirm this cell-intrinsic abnormality in vivo, we conducted bone marrow chimera experiments by transfusing a mixture of equal parts of wild-type (Ly5.1$^+$) and mutant (Ly5.2$^+$) bone marrow cells into lymphocyte-deficient *Il2rg*$^{-/-}$ mice. Consistent with the in vitro results, Ly5.2$^+$ bone marrow cells of mutant males failed to produce B or NK cells, whereas Ly5.1$^+$ wild-type HPCs fully reconstituted both B and NK cells in the same recipient mice (Fig. 6B). Transplanting wild-type bone marrow cells into irradiated mutant male mice rescued the B and NK cell deficiency (Fig. 6C), and PPs were also recovered 10 wk after the transplant (data not shown). This suggests that the PP deficiency is a result of the B cell deficiency and not an anlage defect. These results clearly indicate that the defect of B and NK cells in the mutant mice was intrinsic to hematopoietic cells.

Interestingly, the in vitro lymphopoiesis of B and NK cells from fetal liver HPCs was the same whether the HPCs were from the mutant males or their female littermates (Fig. 7A). Furthermore, the male fetal liver cells reconstituted B and NK cells in vivo, although at a lower level than cells from female littermates (Fig. 7B). Because fetal liver progenitors from the mutant males could produce B and NK cells, we compared the fetal B cell subsets and NK lymphopoiesis in male and female littermates at E17.5, when IgM$^+$ B cells and iNK are already present in wild-type mice (20, 21). As expected, we did not find a significant difference in the frequency of B or NK cells in the fetal liver of male and female littermate embryos (Fig. 7C). However, both B and NK cells derived from the male fetal liver disappeared by 10 wk after transplantation (data not shown). Nevertheless, the above results provide further evidence that the fetal B and NK cell development in the males was intact and that the NK and B cells detected in 3-wk-old males were generated from fetal liver progenitors.

In addition, male fetal liver cells could produce these lymphocytes even in male recipients (data not shown), supporting the conclusion that androgen does not contribute to the defect of B and NK cells in these mutant male mice.

EBF restores the precursor cells' ability to generate B220$^+$ B cells in mutant males

To address the molecular mechanisms for arresting the B cell development, we isolated prepro-B cells (Hardy fraction A) from the

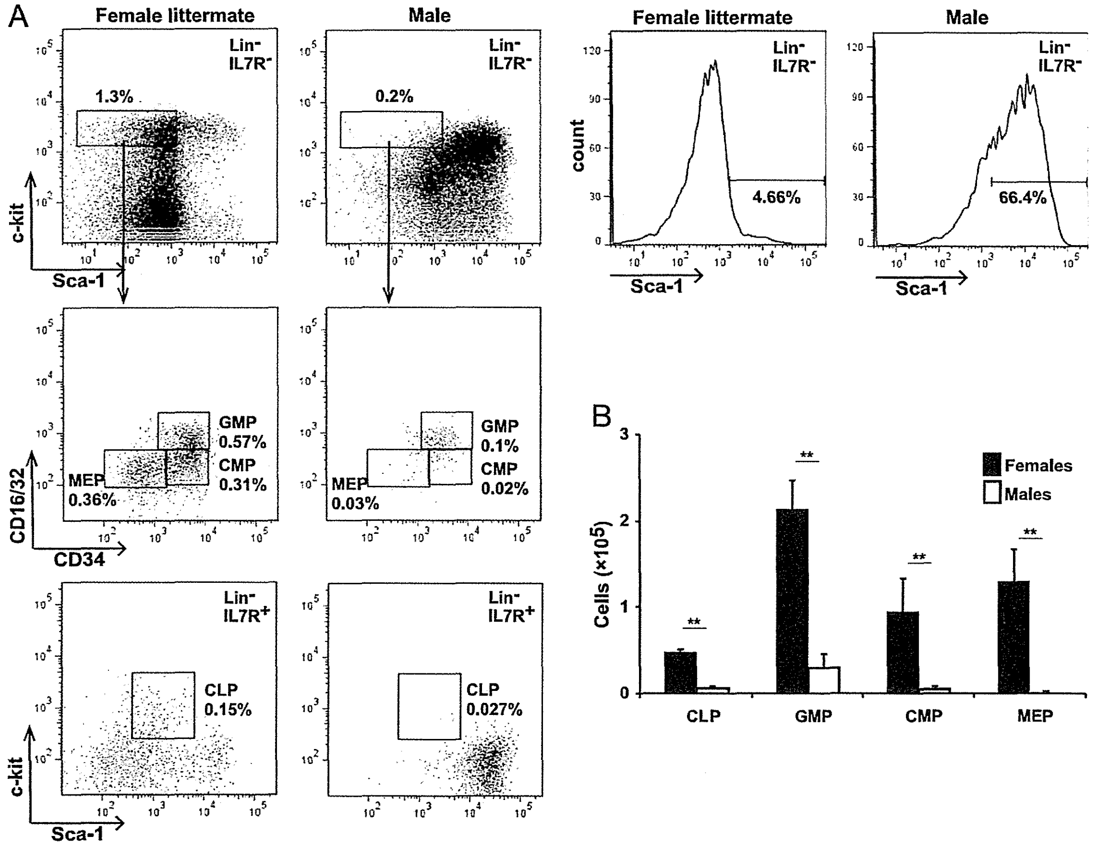

FIGURE 5. Abnormally high expression of Sca-1 on hematopoietic cells in the bone marrow. (**A**) Representative FACS analysis with the bone marrow cells from 12-wk-old mice are shown. Numbers in the FACS plots indicate the percentages of the indicated populations among total bone marrow cells. Each progenitor population was defined as bellow. The histogram shows expression of Sca-1 related to Lin$^-$CD127$^-$ gated cells. (**B**) The average absolute numbers of the indicated populations in the bone marrow are shown ($n = 3$ each). CLP: Lin$^-$CD127$^+$Sca1^{lo}c-Kit^{lo}; CMP: Lin$^-$CD127$^-$c-Kit^{hi}Sca1$^-$CD34$^{+/lo}$CD16/32^{int}; GMP: Lin$^-$CD127$^-$c-Kit^{hi}Sca1$^-$CD34$^+$CD16/32$^+$; and MEP: Lin$^-$CD127$^-$c-Kit^{hi}Sca1$^-$CD34$^-$CD16/32$^-$. $^{**}p < 0.01$.